Skeletal anatomy of the early Permian parareptile Delorhynchus with new information provided by neutron tomography

Dylan C. T. Rowe[1,2], Joseph J. Bevitt[3] & Robert R. Reisz[1,2]

[1]Department of Biology, University of Toronto Mississauga, Mississauga, ON, Canada,

[2]International Centre of Future Science, Dinosaur Evolution Research Center, Jilin University, Changchun, China

[3]Australian Centre for Neutron Scanning, Australian Nuclear Science and Technology Organization, Sydney, NSW, Australia

Corresponding Author:

Dylan Rowe[1]

University of Toronto Mississauga, Mississauga, Ontario, L5L 3H9, Canada

Email address: dylan.rowe@mail.utoronto.ca

Abstract

19 Detailed description of the holotype skeleton of *Delorhynchus cifellii*, made possible through the
20 use of neutron tomography has yielded important new information about the cranial and
21 postcranial anatomy of this the early Permian acleistorhinid parareptile. Hitherto unknown
22 features of the skull include a sphenethmoid, paired epipterygoids and a complete
23 neurocranium. In addition, the stapes has been exposed in three dimensions for the first time in
24 an early parareptile. Postcranial material found in articulation with the skull in this holotype
25 allows for the first detailed description of vertebrae, ribs, shoulder girdle and humerus of an
26 acleistorhinid parareptile, allowing for a reevaluation of the phylogenetic relationships of this
27 taxon with other acleistorhinids, and more broadly among parareptiles. Results show that
28 *Delorhynchus* is recovered as the sister taxon of *Colobomycter*, and 'acleistorhinids' now
29 include *Lanthanosuchus*.

Introduction

32 The reptilian clade known as Parareptilia was first erected by Olson (1947) as one of
33 two subclasses of reptiles. In Tsuji & Muller (2009), Parareptilia was previously defined
34 as the most inclusive clade containing *Milleretta rubidgei* and *Procolophon trigoniceps*
35 (Tsuji & Müller, 2009). The fossil record indicated that parareptiles originated within the
36 late Carboniferous (Modesto et al., 2015), diversified into numerous morphotypes during
37 the Permian and persisted into the Triassic (MacDougall, Brocklehurst & Fröbisch,
38 2019). The body plans exhibited by members of Parareptilia in the early Permian
39 included the bipedal herbivorous bolosaurids, highly specialized aquatic mesosaurs and
40 insectivorous acleistorhinids (Berman et al., 2000; Modesto, 2006; Modesto, Scott &
41 Reisz, 2009).
42   One of the most important locales for understanding the early stages of parareptile
43 evolution is the Richards Spur locality in Oklahoma. Over forty distinct tetrapod taxa
44 have been discovered here, including nine described members of the Parareptilia
45 (MacDougall et al., 2017a). These include the basal parareptile *Microleter mckinzieorum*
46 (Tsuji, Müller & Reisz, 2010), the bolosaurid *Bolosaurus grandis* (Reisz, Barkas & Scott,
47 2002), the nyctiphruretid *Abyssomedon williamsi* (MacDougall & Reisz, 2014), the
48 lanthanosuchoid *Feeserpeton oklahomensis* (MacDougall & Reisz, 2012) and the
49 acleistorhinids *Colobomycter pholeter*, *Delorhynchus priscus*, *D. cifellii*, *C. vaughni* and
50 *D. multidentatus* (Vaughn, 1958; Fox, 1962; MacDougall & Reisz, 2012; Reisz,
51 MacDougall & Modesto, 2014; MacDougall, Modesto & Reisz, 2016; Rowe et al., 2021).
52 Early parareptiles are rare in the fossil record, and most occurrences outside of the
53 southern United States are members of the Bolosauridae (Berman, 2000; Reisz et al.,
54 2007; Müller, Li & Reisz, 2008). in the absence of other evidence, it can be stated that
55 Richards Spur was a center for acleistorhinid diversification as almost all members of
56 the Acleistorhinidae are found in Oklahoma. The preservation of such a high taxic
57 diversity of parareptiles suggests that this region was a center of parareptilian
58 diversification in the early Permian, especially for acleistorhinids (MacDougall, Modesto

59 & Reisz, 2016). Most of the early parareptilian taxa from this locality are known from
60 cranial material, with the exception of the holotype of *D. cifellii* which was preserved with
61 a partial vertebral column and shoulder girdle (Reisz, MacDougall & Modesto, 2014).
62 This holotype is the first known articulated skeleton of an acleistorhinid parareptile. The
63 genus of *Delorhynchus* was originally based upon a partial maxilla as *D. priscus* (Fox,
64 1962). Subsequent studies pertaining to *D. cifellii* include the description of a skull with
65 preserved insect cuticle (Modesto, Scott & Reisz, 2009), as well as a ontogenetic
66 growth series of the jugal and a thorough description of mandibular elements (Haridy et
67 al., 2016; Haridy, MacDougall & Reisz, 2018). A third species, *D. multidentatus*, was
68 recently described as the first early parareptile to possess multiple tooth rows (Rowe et
69 al., 2021).
70   The specimen examined in detail within this study is the holotype of *Delorhynchus*
71 *cifellii*, which consists of a mostly complete skull and partial postcrania. The only
72 discernable difference between the genotype, *D. priscus*, and *D. cifellii* is the lack of a
73 well-developed anterodorsal maxillary flange, mainly because the known specimens of
74 *D. priscus* are restricted to maxillary and dentary fragments. *D. cifellii* differs from the
75 third described species, *D. multidentatus* by the presence of a singular dentary tooth
76 row, the absence of an enlarged dentary foramen and larger overall size. In Reisz et al.
77 (2014), OMNH 73362, OMNH 73363 and OMNH 73524 were also used to provide other
78 details of the cranial anatomy and dentition of *D. cifellii* but the holotype was not studied
79 in detail because of the presence of extensive varanopid fossil material and matrix
80 covering much of the skeleton. As a result of the usage of neutron computed
81 tomography (CT), much of the skeleton has been made available for segmentation and
82 the current project has been able to expand significantly on the original description of
83 the holotype.
84

Materials & Methods

86 OMNH 73515 was scanned using micro-CT at the DINGO thermal-neutron
87 radiography/tomography/imaging station (Garbe et al., 2015) located at the 20 MW
88 Open-Pool Australian Lightwater (OPAL) reactor housed at the Australian Nuclear
89 Science and Technology Organization (ANSTO), Lucas Heights, New South Wales,
90 Australia. The methodology of data acquisition follows the procedure of Mays, Bevitt &
91 Stillwell (2017). OMNH 73515 was reconstructed with a voxel size of 45.4 × 45.4 × 45.4
92 μm.
93   The resulting scan of 2017 slices was processed in ImageJ to minimize file size and
94 improve clarity of data, and then modeled using Avizo 3D segmentation software. All
95 figures were compiled in Adobe Photoshop Elements 8.0. The phylogenetic analysis in
96 this study used PAUP 4.0a149, and the matrix from Cisneros et al. (2020) was updated
97 in Mesquite. A bootstrap analysis was conducted with 1000 replicates, with equally
98 weighted and unordered characters and 1 tree saved per step. Where required, new

99 information was acquired by personal examination of specimens. Bremer decal values
100 were not used due to the weakness of the tree, and branches were collapsed if
101 maximum branch length was zero. The tree length is 878 steps and has a consistency
102 index (CI) of 0.2528, which is reduced to 0.2425 without uninformative characters and
103 0.0758 as a rescaled consistency index (RC). Including uninformative characters, the
104 homoplasy index (HI) is 0.7472, and excluding uninformative characters it is 0.7575.
105 Values for the retention index, f-value and f-rato are 0.2999, 7605 and 0.3245
106 respectively.
107
108 **SYSTEMATIC PALEONTOLOGY**
109 PARAREPTILIA Olson, 1947
110 ANKYRAMORPHA deBraga & Reisz, 1996
111 *DELORHYNCHUS* Fox, 1962
112 *DELORHYNCHUS CIFELLII* Reisz et al., 2014
113

Description

115 **General cranial and postcranial proportions.** The skull of OMNH 73515 is
116 approximately 41.2 mm long, with an orbital length of 12.8 mm resulting in a ratio of
117 skull length to orbital length of 3.23 (Fig. 1). Mid-dorsal vertebrae are 4.38 mm long, and
118 consequently the skull is equal to 9.4 vertebrae in length. The humerus is 27.9 mm long,
119 the scapulae have a maximum length of 21.65 mm and a maximum height of 21.75 mm.
120 **Skull Roof.** A slender dorsal process of the right premaxilla has been preserved
121 contacting the adjacent nasal in OMNH 73515 (Fig. 2A, 2C). No other recognizable
122 features of the premaxilla are present due to postmortem erosive processes, but several
123 small fragments have been tentatively identified as part of the premaxilla.
124 The right maxilla is mostly complete, extending from the ventral border of the external
125 nares to the level of the mid orbit (Fig. 2B, 3, 4). There are 23 tooth positions present on
126 this maxilla, similar to that in OMNH 73362 despite its smaller size. However, the
127 premaxillary process of the left maxilla is missing, as well as tooth-bearing positions
128 underneath the dorsal lamina. The posterior process that underlies the left orbit has also
129 broken off of from the rest of the maxilla, but is still closely associated with the rest of
130 the specimen. Shallow foramina dot the anterolateral surface of the maxilla, with a
131 deeper anterolateral maxillary foramen found at the posterior external nares which is
132 typical of early parareptiles. This foramen extends posteromedially into the maxilla and
133 is exposed on its medial surface at the middle of the dorsal lamina. The preserved
134 premaxillary process is short, forming the ventral portion of the external naris. A small
135 ridge extends from the tip of the lateral surface of the premaxillary process to the first
136 tooth position, which would most likely form a contact with the tooth-bearing portion of
137 the premaxilla. On the medial surface of the premaxillary process, a groove extends
138 from the premaxillary process to the posterior orbit with increasing concavity at the

139   anterolateral maxillary foramen. The external nares are also completely bordered
140   posteriorly by the dorsal lamina. As with *Colobomycter pholeter*, *C. vaughni* and
141   *Acleistorhinus pteroticus* (deBraga & Reisz, 1996; Modesto, 1999; MacDougall,
142   Modesto & Reisz, 2016), an anterolateral projection of the dorsal lamina contributes to
143   the posterodorsal external nares. In contrast, *Karutia fortunata* lacks prominent anterior
144   projections of the dorsal lamina (Cisneros et al., 2020). Towards the maxilla-palatine
145   contact, the tooth-bearing portion of the maxilla is thickened, which extends to the
146   anterior corner of the orbit. Of the maxillary tooth positions, only eleven teeth in the right
147   maxilla are complete, with broken or missing teeth comprising the remaining thirteen
148   positions. None of the teeth in the left maxilla are complete, and only seventeen
149   positions are preserved due to the missing premaxillary process. Posteriorly, the maxilla
150   underlies with the ventral surface of the jugal as a thin terminal process but does not
151   contact with the quadratojugal. The anatomy of the teeth have been previously
152   described in MacDougall et al. (2014) as generally conical with little recurvature distally
153   on the crown. Dentition of the maxilla is largely homodont in shape and isodont in size,
154   with the teeth in the mid-region of the maxilla being only slightly enlarged than the rest
155   of the rest of the tooth row. As expected, posterior maxillary teeth tend to decrease in
156   crown height near the terminus of the bone. The tooth crowns carry delicate mesial and
157   distal cutting edges, and the lingual surfaces have very delicate longitudinal striations.
158   The nasal is a paired element narrow anteriorly where it connects to the premaxilla
159   and broader posteriorly where it connects to the maxilla and lacrimal laterally, as well as
160   the prefrontal and frontal dorsally (Fig. 2A, 2B, 4). Its overall shape is comparable to
161   that of *Acleistorhinus pteroticus* (Daly, 1969). It is possible to discern that a large
162   anterolateral shelf that also forms the dorsomedial border of the external nares, similar
163   to what is seen in *C. pholeter* (MacDougall et al., 2017b). Immediately posterior to the
164   anterolateral shelf, a thickened region of the nasal supports the anterolateral process of
165   the maxillary dorsal lamina. Towards the tip of the snout, a small gap in the
166   anteromedial surface of the nasal provides a short suture for the dorsal process of the
167   premaxilla. The posterolateral surface of the nasal contacts the anterior lateral exposure
168   of the lacrimal. Another smooth suture between the nasal and the prefrontal extends
169   posteromedially on the dorsal surface towards the midline of the skull. On the ventral
170   surface of the nasal, the medial surface is smooth, only slightly concave and extends to
171   the opening of the external nares. This smooth medial surface is bordered laterally by a
172   shallow longitudinal ridge on each side extending into the frontal, with one set of paired
173   foramina at the middle of the ridge. It is likely that this ridge contained the orbitonasal
174   vein. Small, shallow foramina dot the otherwise smooth surface of the nasal.
175   OMNH 73515 has a partially preserved septomaxilla on the right side of the snout,
176   whereas on the left side it has been lost due to postmortem fragmentation. What
177   remains of the septomaxilla contacts the premaxillary process of the maxilla and the
178   anterolateral shelf of the nasal (Fig. 2B, 4B), similar to what is present in *Acleistorhinus*

179   *pteroticus* and *Colobomycter pholeter* (Daly, 1969; MacDougall et al., 2017b). It is
180   unclear, based on the extent of preservation, whether a septomaxillary foramen would
181   be present as in *C. pholeter* (MacDougall et al., 2017b).
182   The lacrimal possesses two lateral exposures on the external surface of the snout – a
183   posterior exposure forming the anterior corner of the orbit, and a smaller anterior
184   exposure between the maxilla and the nasal (Fig. 2B, 4B). This unusual feature, with a
185   significant portion of the bone being covered on the external surface of the snout, was
186   first described in *Colobomycter pholeter* and appears to be present in *Karutia fortunata*
187   (MacDougall et al., 2017b; Cisneros et al., 2020). The double exposure noted in these
188   acleistorhinids appears to be absent in *C. vaughni* where the dorsal lamina of the
189   maxilla and the anterior part of the prefrontal overlies any anterior exposure
190   (MacDougall, Modesto & Reisz, 2016). According to the description of *Acleistorhinus*
191   *pteroticus* (deBraga & Reisz, 1996), the presence of a secondary lateral exposure of the
192   lacrimal is not noted, but that area of the skull roof was damaged and fragmented on
193   both sides, and such a small portion of the lacrimal is difficult to identify.
194   The internal surface of the lacrimal is much more extensive than the laterally exposed
195   surface, and the well-developed anterior process of the lacrimal heavily buttresses the
196   dorsal lamina of the maxilla (Fig. 4B). This medial surface of the lacrimal appears to be
197   a continuation of the robust region of the nasal supporting the anterolateral process of
198   the maxillary dorsal lamina, as the anteromedial portion of the lacrimal merges with this
199   surface of the nasal. Two pairs of lacrimal puncti are present on the thickened orbital
200   surface of the lacrimal, a smaller dorsal punctum and a larger ventral punctum. The
201   lacrimal canal extends from these lacrimal puncti and is bordered entirely by the
202   posterior half of the anterior lacrimal. Anteriorly, the lacrimal canal continues into the
203   maxilla and merges with the external nares. According to MacDougall, Modesto & Reisz
204   (2016),, the lacrimal duct is bordered by the lacrimal posteriorly and the maxilla
205   anteriorly, but the lacrimal does not extend forward anteromedially. Laterally, the
206   lacrimal duct is enclosed by the maxilla. Below the lacrimal puncti, the lacrimal contacts
207   the palatine in a smooth suture. On the medial surface of the posterior lacrimal, a tall
208   ridge extends posteromedially on each side from the anterior corner of the orbit. This
209   antorbital wall has been previously noted to be present in procolophonids such as
210   *Procolophon* and *Owenetta* (Carroll & Lindsay, 1985; Reisz & Scott, 2002), as well as
211   *Macroleter* (Tsuji, 2006). In comparison to the aforementioned parareptiles, the
212   antorbital wall is considerably taller and more slender in *Delorhynchus cifellii*. The
213   posterior portion of the lacrimal also extends into the ventral edge of the orbit above the
214   pronounced dorsomedial channel of the maxilla, terminating at the anterior process of
215   the jugal.
216   The right jugal is complete and articulated in OMNH 73515, suturing onto the maxilla
217   anteroventrally, the pterygoid medially and the postorbital posteriorly (Fig. 2B, 4). On
218   the left side of the skull roof, the left jugal has been disarticulated posterolaterally by

219   postmortem fragmentation, with the posterior edge and processes missing, but is
220   articulated with the maxilla via its slender suborbital process. As mentioned previously,
221   the anterior process of the jugal also has a point contact with the posterior process of
222   the lacrimal. While the posterior process of the jugal does not contact the squamosal as
223   noted in Haridy et al. (2016), the posterolateral skull roof is partially disarticulated and it
224   is possible that the jugal would connect with the squamosal. The posterior process of
225   the jugal does not contact the squamosal in this specimen, which matches what has
226   been suggested in Haridy et al. (2016). Concave, jagged emargination of the
227   posterodorsal process of the jugal forms the anterior border of the temporal fenestra.
228   The latter can be divided into dorsal and ventral regions due to the posterior processes
229   of the jugal. As previously described in Reisz et al. (2014), paired, wedge-shaped alary
230   processes extend medially to contact the pterygoid in a fully articulated individual.
231   Multiple shallow dimples dot the lateral surface of the jugal, which are less pronounced
232   than in *Colobomycter vaughni*, *C. pholeter* and *Acleistorhinus pteroticus* (deBraga &
233   Reisz, 1996; MacDougall, Modesto & Reisz, 2016; MacDougall et al., 2017b) but are
234   similar in their overall pattern.
235   The prefrontal is a relatively large element, extending laterally from the midpoint of
236   the maxillary dorsal lamina to the top of the orbital rim. It is ornamented externally with
237   pronounced tuberosities and deep circular dimples (Fig. 2A, 2B, 4). Anteriorly a small,
238   curved suture occurs between the underlying anterior plate of the prefrontal and the
239   posterolateral end of the nasal. This anterior plate also sutures onto the medial surface
240   of the anterior process of the lacrimal and the posterior half of the dorsal lamina of the
241   maxilla. The antorbital wall originating in the lacrimal extends into the prefrontal but is
242   significantly thinner and taller in this element. This wall is also present in *Colobomycter*
243   *pholeter* (MacDougall et al., 2017b) as well as the bolosaurid *Belebey vegrandis* (Reisz
244   et al., 2007). A shallow fossa is present on the anterior surface of the antorbital wall,
245   composed of the lacrimal and prefrontal, which has been described in *C. pholeter* but
246   not *C. vaughni* (MacDougall, Modesto & Reisz, 2016). Where the prefrontal and lacrimal
247   suture to each other on this ridge, the prefrontal also forms a thin jagged contact with
248   the palatine.
249   The frontal is a narrow and roughly rectangular element extending anteroposteriorly
250   along the skull roof, with a medial suture between the two sides forming a jagged
251   tongue-and-groove pattern (Fig. 2A, 2B, 4A) that is most pronounced in the midorbital
252   region. While the external dorsal portion of the nasal-frontal suture extends obliquely
253   from the midline of the skull, as described in *Acleistorhinus pteroticus* (deBraga & Reisz,
254   1996), the ventral internal portion is linear and extends transversely to the midline of the
255   skull. In addition, the nasal-frontal sutures are somewhat asymmetrical, where the
256   suture on the right side is more lateral in direction than the left, but the overall pattern
257   remains the same, in contrast to what is described in *Colobomycter pholeter* (Modesto
258   & Reisz, 2008). The shallow anterior ridge that runs along the ventral surface of the

259 bone and likely contained the orbitonasal vein appears to end at the anterior orbit,
260 although it remains longitudinal in direction. The prefrontal-frontal suture appears fairly
261 simple on the external surface of the skull, and extends largely anteroposteriorly,
262 curving laterally at its posterior end towards the orbit. A lateral supraorbital flange of the
263 frontal separates the prefrontal and postfrontal, which is thin on both the dorsal and
264 ventral surfaces. The posterior sutures of each side of the frontal are V-shaped on their
265 dorsal surface, as with *C. vaughni* (MacDougall, Modesto & Reisz, 2016). The dorsal
266 surface of the frontal is decorated by multiple prominent tuberosities and dimples. On
267 the ventral surface of the skull, the frontal not only contributes to the anterior orbital
268 ridge but also forms a concavity together with the prefrontal where the eye likely would
269 have resided. Moreover, the frontal contribution to the anterior orbital ridge is
270 contiguous with a pronounced ridge that extends longitudinally to the parietal. This ridge
271 creates a deep concave channel on the ventral surface of the skull roof, likely
272 separating the eye from the olfactory tract.
273   In contrast to the relative complexity of the frontal and prefrontal bones, the
274 postfrontal is a relatively simple sheet-like bone on the dorsal surface of the skull,
275 sutured anteriorly and medially to the frontal and posteriorly to the parietal and
276 postorbital bones. In OMNH 73515, the postfrontal is partially preserved as a thin
277 fragment on the left side of the skull and completely preserved on the right side (Fig. 2A,
278 2B, 4A). As described for *Colobomycter vaughni* (MacDougall, Modesto & Reisz, 2016),
279 this posterodorsal element of the orbit is largely triradiate in outline with anterior,
280 posterior and ventral processes. While the dorsal contact with the frontal is uneven and
281 diagonal, the ventral portion of the anterior postfrontal extends almost to the prefrontal
282 as a circular plate. As with the prefrontal and frontal, the postfrontal is dotted with
283 tuberosities and dimples.
284   The postorbital bridges the dorsal and lateral surfaces of the skull roof and extends
285 ventrally along the posterior orbital edge. Damage to the posterior region of the skull
286 roof on the left side has resulted in an entirely disarticulated postorbital. The only
287 identifiable fragment of the left postorbital is lying in the respective orbit. On the right
288 side, the postorbital is complete and articulated with the postfrontal in an uneven suture
289 pointing towards the pineal foramen (Fig. 2A, 2B, 4). The suture between the postorbital
290 and the dorsal edge of the jugal is smooth, with the lateroventral edge of the postorbital
291 contributing to the temporal fenestra. This contribution to the dorsal edge of the
292 temporal fenestra apparently distinguishes it from what is observed in *Colobomycter*
293 *pholeter* and *C. vaughni* (MacDougall, Modesto & Reisz, 2016; MacDougall et al.,
294 2017b), as well as in *Acleistorhinus* (deBraga & Reisz, 1996). Ornamentation of the
295 dorsolateral surface of the postorbital is considerably more pronounced on the
296 postorbital than in more anterior skull roof elements, with larger tuberosities and several
297 deep dimples. The ventromedial surface is smooth, except for one small foramen
298 immediately behind the posterior border of the orbit.

299   The parietal is broadly hexagonal in outline, and is bordered by the frontal anteriorly,
300   the postfrontal anterolaterally and the postorbital laterally (Fig. 2A, 4A). The interparietal
301   suture is tongue-and-groove in appearance, similar to the interfrontal suture but less
302   jagged and uneven. A notable tongue-like projection of the left parietal overlies the right
303   parietal and forms much of the anterior border of the pineal foramen. The large pineal
304   foramen is located near the middle of the interparietal suture, similar to the condition
305   seen in *Colobomycter pholeter* (MacDougall et al., 2017b). This condition contrasts to
306   what is described in *Acleistorhinus pteroticus*, where the pineal foramen is positioned
307   anteriorly in the interparietal suture (deBraga & Reisz, 1996). The jagged fronto-parietal
308   suture extends along the posterior half of the orbit, with the parietal underlying the
309   frontal significantly. Lateral parietal-postfrontal and parietal-postorbital sutures are
310   wavelike, with a tongue-and-groove pattern similar to the interparietal suture. A groove
311   on the posterolateral side of each side of the parietal would also underly the
312   supratemporal. On the dorsal surface, tuberosities and dimples ornament the parietal in
313   the same way as other dorsal skull elements. The posterior occipital surface of the
314   parietal is relatively smooth, curving posterolaterally towards the parietal-supratemporal
315   suture, and would most likely form attachment points for neck musculature. In contrast
316   to the dorsal surface of the bone, the ventral surface is mostly smooth and slightly
317   concave, with the exception of the ridged area adjacent to the ventral longitudinal ridge
318   of the frontal, a posterior continuation of the massive ridge of the ventral surface of the
319   latter bone. Several tiny foramina are present near the suture with the frontal. A shallow
320   extension of the fronto-parietal ridge curves towards and terminates at the pineal
321   foramen, but connect to very slender, lip-like flanges that form the ventrolateral edges of
322   the foramen, and approach each other posteriorly. An additional pair of foramina occurs
323   centrally on each side of the parietal, near the pineal foramen.
324   The postparietals are present and well-preserved along the skull midline in
325   articulation with the parietals in OMNH 73515, suturing onto the parietal anteriorly and
326   primarily contributing to the occipital surface of the skull (Fig. 2A, 4A). While the tiny
327   skull roof contribution of the postparietal is bulbous, the occipital surface of the
328   postparietal is concave and slightly rugose. In contrast, the ventral surface of the
329   postparietal is relatively smooth. The right postparietal appears to be considerably
330   larger than the one on the left, and the bulbous dorsal surface originates from this
331   element but it appears that both elements underlie the parietal and are sutured to the
332   ventral surface of that bone. Ventrally, the postparietals carry a pair of delicate ridges
333   that extend from the posterior region of the parietal, near the pineal foramen, and are
334   marked by the presence of a slender anterior process. These ridges broaden out as
335   they extend into the main body of this element. The left tabular is complete and
336   articulated with the posterolateral left parietal in OMNH 73515 but does not contact any
337   other elements. It is very small and unornamented and would join with the parietal-
338   supratemporal suture laterally in a fully articulated specimen.

339   The squamosal is a fairly large, heavily sculptured component of the skull roof that
340   contacts the postorbital and the supratemporal medially, contributes to the border of the
341   temporal opening anteriorly and overlies the quadratojugal ventrally. The right
342   squamosal is nearly complete and articulated with the adjacent postorbital in OMNH
343   73515, but the left squamosal is very fragmented and has not been rendered (Fig. 2A,
344   2B, 4). This posterior skull roof element is trapezoidal with weakly convex and concave
345   posterior and anterior margins. The ventral margin of the squamosal extends
346   posteroventrally where it contacts the dorsal process of the quadratojugal. The
347   anterodorsal margin of the squamosal forms a straight contact with the postorbital,
348   curving around a large tuberosity in the middle of the squamosal. At the dorsal border of
349   this element, a small shelf extends dorsally that underlies the postorbital and would
350   underly the supratemporal in a fully articulated specimen. This ridge continues onto the
351   posterior surface, where it wraps around to the occipital region as in *Colobomycter*
352   *pholeter* (MacDougall et al., 2017b). Posteroventrally, the ridge also contributes to the
353   dorsal border of the quadrate foramen.
354   As in most parareptiles the quadratojugal is tall and occupies a significant portion of
355   the postorbital region of the skull roof. As with the squamosal, the right quadratojugal of
356   OMNH 73515 is complete and partially articulated while the left is heavily damaged (Fig.
357   2A, 2B, 4B). If the right quadratojugal were fully articulated, it would suture onto the
358   squamosal dorsally, the jugal anteriorly and the quadrate medially. The anterior process
359   of the quadratojugal is triangular in shape, contributing to the ventral surface of the skull
360   as well as a slightly jagged posteroventral border of the temporal fenestra. While the
361   quadratojugal possesses tuberculous ornamentation on the lateral surface, it is much
362   less pronounced than its neighbouring elements. In contrast, the external surface of the
363   occipital flange that contributes to the quadrate foramen, as well as the process
364   supporting the lateral condyle of the quadrate, is smooth.. A small foramen is present on
365   the dorsomedial surface of the quadratojugal, but otherwise the internal surface is
366   smooth.
367   The supratemporal is also a major component of the posterolateral region of the skull
368   roof, but due to postmortem fragmentation the left supratemporal is missing from OMNH
369   73515 (Fig. 4A). The right supratemporal is disarticulated and only partially preserved,
370   but still associated with the specimen at the lateroventral right corner of the occipital
371   surface. On its dorsal surface, the supratemporal is adorned with short, wide
372   tuberosities, whereas the ventral surface is smooth and slightly concave. This element
373   forms much of the posteroventral skull roof and is underlain by the parietal medially, the
374   postorbital anteriorly and the squamosal laterally with particularly large facets of
375   articulation on the parietal bone. While the supratemporal appears to readily fall off
376   postmortem in many acleistorhinids, it clearly demonstrates that this bone made a
377   significant contribution to the ventral skull roof surface. This extensive ventral skull roof
378   contribution contribution is observed in *Macroleter* and *Owenetta* (Reisz & Scott, 2002;

379 Tsuji, 2006), indicating that this is a widespread condition in parareptiles, in contrast to
380 its restricted contribution or absence in eureptiles and most synapsids.
381 **Palate.** In *Delorhynchus cifellii*, the palate is comprised of four dentigerous elements –
382 the vomer, the palatine, the pterygoid and the ectopterygoid (Fig. 5). Much of the ventral
383 palatal surface is covered by fields of teeth arranged in distinct groups that extend over
384 several bones and separated from each tooth by slightly concave areas and distinct
385 large grooves. Anteriorly, the choana is long and slender, separating the vomer from the
386 maxilla and ending posteriorly at the curved lateral process of the palatine bone.
387 Remarkably, the choana is connected posteriorly to a wide groove that extends
388 posterolaterally along the ventral surface of the palatine from the choana parallel to the
389 tooth row and the lateral edge of the palatine. This groove changes direction at the
390 palatine-ectopterygoid suture and continues in a posteromedial direction across the
391 ventral surfaces of the ectopterygoid and pterygoid. Posteriorly, this groove separates
392 the dental field of the transverse flange and its posterior continuation on the quadrate
393 ramus of the pterygoid from the basicranial articulation. It is possible that this groove
394 extending from the choana into the throat region may represent an air passage that
395 allowed for respiration even when the palatal dentition was engaged in holding prey.
396   The vomer is triangular in outline, forming the anterior tip of the palatal region(Fig. 5).
397 This palatal element is bordered posterolaterally by the palatine and posteromedially by
398 the narrow anterior process of the pterygoid, with the palatine-vomer suture at the level
399 of the interpterygoid vacuity as seen in *Acleistorhinus* (deBraga & Reisz, 1996). Two
400 fields of vomerine teeth are present on the ventral surface, with a narrower lateral field
401 and a wider medial field as seen in other acleistorhinids as well as in *Macroleter* and
402 *Saurodektes* (Reisz & Scott, 2002; Tsuji, 2006). Where the tooth rows converge at the
403 anterior terminus, the teeth are comparatively larger in size as described in
404 *Colobomycter pholeter* and *Macroleter* (MacDougall et al., 2017b). Much of the dorsal
405 surface is smooth, except for an alar flange that connects to the orbitonasal ridge of the
406 palatine. In contrast to *Macroleter* and *Captorhinus laticeps* (Heaton, 1979; Tsuji, 2006),
407 the alar flange is entirely straight, forming the medial border of the internal nares. A well
408 developed, tall medial flange is an anterior extension of a similar flange along the
409 medial edge of the pterygoid, and extends anteriorly to the premaxilla. This flange forms
410 a relatively thick suture between the left and right vomers.
411   As with *Colobomycter pholeter* (MacDougall et al., 2017b), much of the lateral part of
412 the palate consists of the palatine (Fig. 5). This element is bordered by the vomer
413 anteromedially, forming the posterior choana, and contacts the pterygoid medially and
414 the ectopterygoid posterolaterally. The lateral contact between the ectopterygoid and
415 palatine is interrupted by the suborbital foramen, which is modest on the left side and
416 widened on the right side by a small hole. A large dental field is present diagonally
417 along much of the length of the palatine and extends onto the pterygoid as with other
418 acleistorhinids (deBraga & Reisz, 1996). This field widens considerably along its length,

419   decreasing in the size of the teeth posteriorly but increasing in density. A wide groove
420   with a smooth surface extending from the posterior choana is bordered medially by this
421   tooth field, and laterally by a thickened ridge contacting the maxilla. On its dorsal
422   surface, the alar flange continues into the transverse orbitonasal ridge as seen in
423   *Captorhinus laticeps* and *Macroleter poezicus* (Heaton, 1979; Tsuji, 2006). These two
424   ridges are tallest at their contact, suturing onto the lacrimal and prefrontal. A shallow,
425   wide ridge extends posterolaterally, sutured to the maxilla.
426   The ectopterygoid is a relatively large element of the palate, bridging a large gap
427   between the posterior region of the palatine and the transverse flange of the pterygoid.
428   Both ectopterygoids are present in OMNH 73515 and complete, but the right
429   ectopterygoid is slightly disarticulated (Fig. 5A, 5C). This element is broadly triangular,
430   suturing onto the palatine anteromedially, the pterygoid posteromedially and the maxilla
431   laterally. The wide groove extending from the ventral surface of the palatine curves
432   sharply on the ectopterygoid, continuing posteromedially into the pterygoid. This groove,
433   likely serving as an air passage, is bordered by several palatal teeth medially and by
434   thickened contacts with the maxilla and jugal laterally. Palatal teeth are present on the
435   ectopterygoid as part of the relatively wide field in this region of the palate, which differs
436   from the condition described in both *Colobomycter pholeter* and *Acleistorhinus*
437   *pteroticus* (deBraga & Reisz, 1996; MacDougall et al., 2017b). The dorsal surface is
438   mostly smooth, with a shallow ridge resulting from the canal.
439   The pterygoid is the largest element of the palate as with most early Permian
440   amniotes, including acleistorhinids, with a broadly triangular shape (Fig. 5). This
441   element possesses a mostly broad, flattened palatal process, a concave transverse
442   process and a quadrate ramus extending posterolaterally. The anterior palatal process
443   extends anteriorly to the vomer and palatine, separating the posterior half of the
444   vomers. Two fields of teeth are present on this anterior process, with one anterolateral
445   field extending from its central portion onto the palatine and an anteromedial field. The
446   anteromedial field of teeth can be subdivided into a row that extends along the medial
447   edge of the bone where the interpterygoid vacuity is located, and a secondary row that
448   extends roughly parallel to the medial row. This pattern resembles what is seen in
449   *Colobomycter* (MacDougall et al., 2017b). The transverse flange is a robust feature of
450   the bone, and it extends an edentulous process anterolaterally towards the medial
451   process of the jugal, with a thin bifurcating sutural contact with the latter. The rest of the
452   ventral surface of the transverse flange is highly dentigerous, with a row of large teeth
453   on the posteroventral edge of the transverse process as well numerous smaller teeth as
454   in *C. pholeter* (MacDougall et al., 2017b). Anteromedially, the transverse flange borders
455   the broad groove that separates the dentigerous portion of the flange from the palatal
456   region of the pterygoid, and both the transverse flange and the groove extend
457   posteromedially into the quadrate ramus. In contrast to the anterior and transverse
458   processes, the quadrate ramus is relatively smooth and curves posterolaterally to cup

459   the quadrate. As in other acleistorhinids, the row of marginal teeth present on the
460   posterior edge of the transverse flange continues into the quadrate ramus, decreasing
461   in size as they go along. The dorsal surface of the pterygoid is less complicated, with
462   two noteworthy features: a paired medial ridge extending dorsally from the tip of the
463   anterior process to the orbital region where the sphenethmoid is located, and a groove
464   and sutural area in the region of the basicranial articulation for attachment of the
465   epipterygoid ossifications, which are preserved in articulation. Posterodorsally, a
466   tympanic ramus is present on the quadrate flange of the left pterygoid.
467   The morphology of the epipterygoid, while comparatively more delicate, resembles
468   the condition seen in *Macroleter poezicus* (Tsuji, 2006). Anteroventrally, the base of the
469   epipterygoid contributes with the pterygoid to the articular surface of the basicranial
470   articulation, while posteriorly it overlies the anteromedial quadrate ramus of the
471   pterygoid (Fig 5B). The dorsal process of the epipterygoid, preserved in its entirety,
472   extends as a slender pillar posteromedially.As with the quadrate ramus of the pterygoid,
473   the surface of the epipterygoid is smooth.
474   In *Delorhynchus cifellii*, the parasphenoid and basisphenoid are fused together and
475   henceforth are referred to as the parabasisphenoid, with specific features that can be
476   identified as part of the parasphenoid and basisphenoid will be described separately.
477   The parabasisphenoid is unusually large and occupies the posterior half of the palatal
478   surface, whereas in *Acleistorhinus pteroticus* it appears relatively shorter and occupies
479   only one third of the palatal length (deBraga & Reisz, 1996). As with *A. pteroticus* and
480   *Colobomycter pholeter* (MacDougall et al., 2017b), this posteroventral palatal element is
481   triangular in outline (Fig. 5C, 6). A narrow, short cultriform process extends anteriorly,
482   and overlies the interpterygoid vacuity. Given the length of the cultriform process, the
483   anteriormost extent of the interpterygoid vacuity was not bisected by the cultriform
484   process. Where the cultriform process merges with the rest of the parabasisphenoid,
485   two fields of short teeth are present on the ventral surface. These tooth rows diverge
486   posteriorly resembling the condition seen in *A. pteroticus* and *Lanthanosuchus watsoni*
487   (deBraga & Reisz, 1996). The most lateral rows of teeth are positioned over the cristae
488   ventrolaterales along the main body of the parasphenoid, whereas the most medial
489   rows are present on low ridges as in *L. watsoni* (deBraga & Reisz, 1996). These rows of
490   teeth extend to the level of the posterior termination of the pterygoid teeth on the
491   quadrate ramus. Unlike *A. pteroticus*, the tooth rows also extend anterolaterally to
492   overly the basisphenoid rostrum and posterior cultriform process. The basipterygoid
493   processes extend anterolaterally and would form synovial joints with the basicranial
494   recesses. As in *Macroleter poezicus* (Tsuji, 2006), the sella turcica is positioned
495   caudally to the dorsal body, bordered by the clinoid processes posterolaterally. The
496   medial and lateral surfaces of each clinoid process is smooth, and the foramen for
497   cranial nerve VI pierces each process posterodorsally. . Transversely, the clinoid

498 processes are connected by a thin dorsum sellae. A pair of ridges overly the cristae
499 ventrolateralis and extend posterolaterally.
500   Both quadrates are preserved in the holotype, with the right element in articulation
501 with the pterygoid. As in *Acleistorhinus* (deBraga & Reisz, 1996), the quadrate is short
502 anteroposteriorly, overlying the lateral quadrate ramus of the pterygoid as a thin triangle
503 of bone (Fig. 4), and with a massive transversely oriented condyle. The quadrate is
504 slender anteriorly but thickens considerably as it extends posteriorly, contributing to the
505 ventral border of the quadrate foramen and suturing onto the quadratojugal laterally.
506 Posterolaterally, the quadrate underlies the quadratojugal as a massive process. As in
507 *Colobomycter pholeter* (MacDougall et al., 2017b), the contact with the articular facet
508 would be secure in a fully articulated individual, with protuberances of the quadrate
509 condyle fitting into the dorsal sockets of the articular. Medially, a short, curved process
510 of the quadrate extends anteromedially, providing an articulating or supporting surface
511 for the stapes. The dorsal process of the quadrate is tall and is exposed occipitally, with
512 a bladelike lateral extension and an open dorsal termination. This process curves
513 medially and separates the squamosal and pterygoid.
514   The sphenethmoid is preserved in this specimen as an elongated Y-shaped sheet of
515 bone, as described in *Captorhinus laticeps* as the interorbital septum (Heaton, 1979).
516 This element is shifted out of place, with the ventral margin partially contacting the
517 cultriform process of the parabasisphenoid (Fig. 5A, 5B, 6). In a fully articulated
518 specimen, the ventral margin of the sphenethmoid would likely contact the trough of the
519 cultriform process. Unlike *Ca. laticeps*, the bifurcation into the sola supraseptales occurs
520 at approximately one-third of the height of the sphenethmoid. The surface of this
521 element is smooth as was described in *Co. pholeter* (Modesto & Reisz, 2008). The sola
522 supraseptales are somewhat damaged, but the preserved margin is thickened dorsally
523 and would likely contact the mediorbital ridge of the prefrontal, frontal and postfrontal as
524 suggested for *Ca. laticeps*. The morphology of the sphenethmoid in *Delorhynchus cifellii*
525 differs considerably from those seen in *Dimetrodon* and *Ophiacodon* (Romer & Price,
526 1940), where the sola supraseptales bifurcate at two-thirds of the height of the element.
527 In addition, the anterolateral surface in these synapsids is noticeably sculptured and a
528 pair of foramina extend anterolaterally through the base of the sola supraseptales,
529 features not shared by *D. cifellii*.
530   The stapes is completely preserved but disarticulated on both sides of OMNH 73515
531 (Fig. 5C, 7). This element is compact and robust, in contrast to the more elongated
532 condition seen in captorhinids such as *Captorhinus laticeps* and *Euconcordia*
533 *cunninghami* (Heaton, 1979; Reisz, Haridy & Müller, 2016) and synapsids such as
534 *Ophiacodon retroversus*, *Dimetrodon limbatus*, *Mesenosaurus romeri* and *Martensius*
535 *bromackerensis* (Romer & Price, 1940; Reisz & Berman, 2001). A large footplate is
536 present as described in *Acleistorhinus pteroticus* (deBraga & Reisz, 1996), with a deep
537 central pit, a thin dorsal edge and a broad ventral edge. The thickness of the footplate

538   rim contrasts to what is observed in *C. laticeps*, where the rim is uniformly thin.
539   Anteriorly, the footplate would contact the basisphenoid and prootic, whereas the
540   posteromedial edge would lie within the stapedial recess of the basioccipital and
541   opisthotic as in *C. laticeps*. The columella is short, broad and distally expanded in dorsal
542   view, with ridges on its anterior, dorsal and ventral surfaces as with C. laticeps. Lateral
543   expansion is observable from an occipital view, as in *Milleretta rubidgei* (Gow, 1972).
544   The robust morphology of the columella differs considerably from the elongated
545   condition seen in captorhinids and synapsids (Romer & Price, 1940; Heaton, 1979;
546   Reisz & Berman, 2001; Reisz, Haridy & Müller, 2016; Berman et al., 2020). Extending
547   from the lateral end of the terminus to the dorsal process is the dorsal process,
548   increasing in height medially and ending in unfinished bone that would likely connect to
549   cartilage, as in *Milleretta rubidgei* (Gow, 1972). The distal columella shares this
550   unfinished texture, connecting to the lateral end of the dorsal process anteriorly, and
551   would contact the quadrate in an interlocking process. Compared to both captorhinids
552   and synapsids, the dorsal process is short and stout, without a pronounced channel for
553   the vena capitis lateralis or the hyoid ramus of the facial nerve. The anterior ridge
554   extends posteromedially from the ventrolateral end of the columella to the base of the
555   footplate, but is not perforated by a dorsoventral foramen as in C. laticeps. The
556   stapedial foramen instead extends anteroposteriorly immediately adjacent to the
557   footplate, as observed in *Mesenosaurus romeri* (Reisz & Berman, 2001). While this
558   foramen is primarily anteroposterior in *O. retroversus* and *D. limbatus*, the orientation is
559   comparatively more posteroventral in orientation (Romer & Price, 1940). It is likely that
560   the stapedial artery was mostly or entirely directed anteroposteriorly.
561   Immediately posterior to the parabasisphenoid, the basioccipital-exoccipital complex
562   forms the occipital condyle in a fully articulated specimen (Fig. 5). The basioccipital is
563   roughly pentagonal in shape, with a thickened posterior surface where it sutures onto
564   the paired exoccipitals. The exoccipitals extend dorsally to form the dorsolateral borders
565   of the occipital condyle and the ventrolateral edges of the foramen magnum. While the
566   columnar shape of these elements generally resembles the condition of *Macroleter*
567   *poezicus* (Tsuji, 2006), the dorsal surface lacks medial and lateral processes. The
568   shape of the paired exoccipitals therefore more closely resembles what is reconstructed
569   for *Saurodektes kitchingorum* by Reisz & Scott(2002).
570   The neurocranial complex consisting of the supraoccipital, opisthotic and prootic
571   complex is fused in *Delorhynchus cifellii* without visible sutures (Fig. 5, 8). The following
572   descriptions of the neurocranium elements therefore reference their probable anatomy.
573   However, features such as the paired posttemporal foramina dividing the supraoccipital
574   and opisthotic and the venous notch allow for some differentiation of individual
575   elements. As with *Macroleter poezicus* (Tsuji, 2006), the supraoccipital is
576   anteroventrally concave, with a low median sagittal ridge and a semicircular crest on the
577   occipital surface. Unlike *Macroleter,* the semicircular crest is bifurcated by the sagittal

578 ridge, which would connect with the ventral corner of the paired postparietals.
579 Occipitally, the supraoccipital is concave and forms the dorsal border of the foramen
580 magnum, with a medial notch resulting in a keyhole shape similar to the condition in
581 *Macroleter* (Tsuji, 2006). Posteriorly, this braincase element includes a pair of wide,
582 flattened indentations that would contact the dorsal exoccipitals. The prootic extends
583 forward as paired, lateromedially curved processes which would contact the
584 basisphenoid as in *Milleretta* (Gow, 1972) and *Macroleter* (Tsuji, 2006). The
585 anterodorsal surfaces of these processes are marked by venous notches, as in
586 *Dimetrodon limbatus* (Romer & Price, 1940) but more pronounced in concavity.
587 Immediately ventral to the venous notches, a pair of foramina extend posteromedially
588 through the middle of the prootic which would have probably enveloped cranial nerve
589 VII as noted in *Milleretta* and *Macroleter*. Dorsally, the prootic is marked by paired
590 cylindrical swellings which envelop the anterior semicircular canals. Interestingly, the
591 largest element in the neurocranial complex is the opisthotic, which expands
592 posterolaterally into dorsal and ventral regions of the paroccipital process. This
593 morphology resembles what is seen in other parareptiles like *Macroleter* and
594 *Acleistorhinus*, where the paroccipital process extends ventrolaterally to the skull roof.
595 On the dorsal region of the paroccipital process, a shallow groove is present which may
596 have connected to the supratemporal and parietal as noted in deBraga and Reisz
597 (1996).
598 Ventrally, the neurocranium is relatively open, with partially ossified channels for the
599 bony labyrinth (Fig. 9). The vestibule was only reconstructed at its contact with the
600 posterior semicircular canal (PSC) due to the disarticulation of the neurocranium and
601 the lack of ossification. Neurocranial morphology indicates that the entire bony labyrinth
602 was tilted posteroventrally. Anteriorly, the prootic encapsulates the majority of the
603 anterior semicircular canals (ASC) and the anterior and lateral ampullae, while
604 posterolaterally the opisthotic envelops the lateral semicircular canals (LSC), the
605 secondary common crus and the lateral region of the posterior semicircular canal. It is
606 likely that the opisthotic would also have encapsulated the vestibule dorsally. The only
607 feature of the bony labyrinth present within the supraoccipital is the common crus and
608 the medial sections of the ASC and PSC. Given the orientation of the neurocranial
609 complex, the ASC would be positioned dorsally even without the curvature of the
610 common crus. Both the ASC and PSC are arcuate, while the LSC is L-shaped.
611 Anterodorsally, the dorsal expansion of the anterior semicircular canal is slight as with
612 varanopids (Bazzana et al., 2021). A secondary common crus is not present, as the
613 LSC extends posteromedially towards the posterior semicircular canal but does not
614 connect with it. Both the angle between the ASC and PSC and the angle between the
615 ASC and LSC are sub-orthogonal, with averaged measurements of 71° and 87°
616 respectively. While the angle between the ASC and the LSC is the same as in

617   *Mesenosaurus*, the angle between the ASC and PSC is less orthogonal than in
618   varanopids (Bazzana et al., 2021).
619   The basihyal and ceratohyals are preserved in OMNH 73515, but are disarticulated
620   from one another (Fig. 5B). The basihyal possesses a semilunate anterior edge and
621   narrows into paired posterior projections, as opposed to the hourglass shape observed
622   in *Saurodektes kitchingorum* (Reisz & Scott, 2002). While the ventral surface is smooth,
623   a pair of rounded protrusions are present on the dorsal surface near the posterior
624   processes. The ceratohyals are elongated and rodlike that expand distally, with slight
625   medial curvature as in *S. kitchingorum*.
626
627   **Mandible.** The anatomy of the lower jaw corresponds to what has been previously
628   described for *Delorhynchus cifellii* (Haridy, MacDougall & Reisz, 2018) The dentary in
629   OMNH 73515 is mostly complete and articulated with adjacent mandibular elements,
630   but a break at the tip of the mandible disarticulates the left side of the mandible from the
631   rest of the skull (Fig. 2C, 10). Anteriorly, the dentary is underlain by the splenial in a
632   relatively smooth suture while the posterolingual dentary sutures onto the angular in a
633   similar pattern. The posterolateral surface of the dentary is adjacent to, and overlies, the
634   anterior surangular. Both coronoid elements are also supported by the dorsomedial
635   surface of the dentary. On the anterior surface of the dentary, the lateral surface is
636   dotted with small foramina, a pattern shared by *Colobomycter* (MacDougall, Modesto &
637   Reisz, 2016), *Karutia fortunata* (Cisneros et al., 2020) and *D. multidentatus* (Rowe et
638   al., 2021). A posterodorsal extension of the dentary extends over the lateral surface of
639   the surangular, a feature not found in other acleistorhinids. The ventrolateral surface of
640   the dentary also bifurcates posteriorly at the contact with the angular. On its medial
641   surface, the dentary forms the lateral border of the Meckelian canal, which is deeply
642   concave resulting in a transverse C-shape. The Meckelian canal widens posteriorly and
643   extends into the posterior mandibular elements. Immediately anterior to the coronoid, a
644   deep foramen branches off from the Meckelian canal. This foramen extends anteriorly
645   directly underneath the dentigerous section of the dentary to the mandibular symphysis,
646   and may have provided blood supply to growing teeth.
647   In this specimen of *Delorhynchus cifellii*, the coronoid complex is complete and
648   articulated on each side of the mandible, with the suture between the anterior and
649   posterior coronoid ossifications clearly visible as first described in Haridy et al. (2018).
650   These ossifications suture onto the junction between the splenial and dentary (Fig. 10A,
651   10B). The dorsal surfaces of the coronoids are covered with shagreens of small, short
652   teeth. As with other specimens of *Delorhynchus cifellii*, as well as *D. multidentatus*, the
653   posterior coronoid ossifications terminate in winglike projections that extend
654   dorsomedially, adjacent to the coronoid process.
655   The splenial underlies the dentary immediately behind the dental symphysis and
656   extends posteriorly to the coronoid process, sheathing the Meckelian canal lingually
657   (Fig. 10). The dorsal splenial-dentary suture directly underlies the coronoid ossifications,

658   diverging at the midpoint of the posterior coronoid and extending posteroventrally
659   towards the lingual surface of the angular. Anterodorsally, the splenial bifurcates into a
660   short dorsal projection and a longer ventral projection that extends to the dental
661   symphysis. The ventral splenial contacts the dentary anteriorly and forms the
662   posteriormost extent of this mandibular element.
663   The angular is a curved sheet extending from the anteriormost coronoid to the
664   articulating surface of the mandible (Fig. 10A, 10B). Examination of the inside of the
665   anterior mandible reveals a thin process of the angular sheathing the Meckelian canal
666   ventrally, which increases in concavity. This process is also covered by the dentary
667   laterally near the intercoronoid suture, where it appears on the lateral surface of the
668   mandible as a triangular process. The posterior angular also extends to the articulating
669   facet of the surangular. Immediately dorsal to the posterior terminus of the splenial, an
670   oval-shaped foramen perforates the lingual surface of the angular. This foramen is
671   bordered by the angular ventrally and the prearticular dorsally, and a small extension of
672   the splenial overlies the anterior edge. The posterior extension of the angular forms the
673   ventral portion of the mandible, curving lingually with a well-sculpted lateral surface. The
674   cup-shaped dorsolingual surface of the angular retains its shape to its posterior
675   terminus, where it sutures the articulating facet of the mandible.
676   As seen in the holotype of *Delorhynchus cifellii*, much of the coronoid process is
677   made up of the surangular (Fig. 10). This dorsal mandibular element underlies the
678   dentary anteriorly as a thin sheet before expanding into the posteriormost labial surface
679   of the mandible. The thin posterior terminus of the dentary overlying the surangular
680   continues into a lateral ridge of the surangular. This ridge extends to the posterior
681   bifurcation of this element, where a lingual extension cups the articular anteriorly. Other
682   than several small foramina near the bifurcation of the surangular, the lingual surface is
683   smooth and laterally convex.
684   The dorsolingual surface of the posterior part of the mandible is covered by the
685   prearticular, which is more heavily sculpted on its lingual surface than most other
686   mandibular elements (Fig. 10A, 10B). Two ridges are present, with an anterior ridge and
687   a well-defined dorsal ridge extending posteroventrally. As with the surangular, the
688   prearticular cups the articular on its posterior terminus. The ventral surface of this
689   element also contacts the angular in a mostly straight suture that curves ventrally under
690   the articular suture. Unlike OMNH 72363 (Haridy et al., 2018), the prearticular does not
691   contact the anterior coronoid, and these differences may be due to ontogeny.
692   The articular is the most heavily built element of the mandible, with a wrinkled
693   external surface (Fig. 10A, 10B). Compared to the thoroughly described articular in
694   *Captorhinus laticeps*, this element is much shorter (Fox & Bowman, 1966). An anterior
695   extension of this element with thin walls forms the posterior wall of the Meckelian canal,
696   although this acuminate extension is shorter than what was seen in *Captorhinus*
697   *laticeps*. As with *Acleistorhinus pteroticus* and *Colobomycter pholeter* (MacDougall et

698   al., 2017b), there are two articulating facets on the posterodorsal surface. Two pairs of
699   foramina can be observed on the lingual articulating facet – a small pair on the posterior
700   surface matching the condition in *A. pteroticus* (Daly, 1969), and a larger pair on the
701   lingual surface.
702   **Postcranium.** The holotype of *Delorhynchus cifellii* includes numerous postcranial
703   elements, permitting a better understanding of the basic acleistorhinid anatomy. A
704   nearly complete atlas-axis complex is present in this parareptile, including a proatlas, as
705   well as other cervical and dorsal vertebrae. A proatlas is preserved in the form of the left
706   proatlantal neural arch, which has been dislodged from its contact with the atlantal
707   neural arch. The oval-shaped plate and thin, posteriorly projecting spine more closely
708   resembles the condition of *Captorhinus aguti* (Fox & Bowman, 1966) than the triangular
709   process present in *Ophiacodon* and *Dimetrodon* (Romer & Price, 1940). Anteriorly, the
710   proatlantal neural arch widens at its shallowly concave contact with the exoccipital.
711   While the general morphology of the proatlantal neural spine resembles *C. aguti*, the
712   spine appears to be slightly more elongated. The postzygapophosis is short and robust,
713   with a rounded, shallowly concave surface similar to the exoccipital-proatlas contact
714   where it would suture onto the atlas. The atlas is preserved but the atlantal neural arch
715   has been disarticulated from the atlantal centrum (Fig. 1B). The atlantal centrum is
716   robust, with short laterally projecting processes which may have partially supported the
717   axial rib as mentioned in Dilkes & Reisz (1986) despite the absence of the axial
718   intercentrum. Dorsally, the atlantal centrum is flattened where it contributes to the
719   vertebral foramen. Posteriorly, the notochordal canal of the atlantal centrum expands
720   posteriorly. Anteroventrally, the foot processes are robust with flattened atlantal
721   prezygapophyses that would support the proatlantal postzygapophyses. Wide, laterally
722   projecting atlantal postzygaphophyses are present on the neural plates of the atlantal
723   neural arch. A pair of bifurcated neural spines project from the postzygapophoses,
724   which are perforated on each side by a small dorsally oriented foramen. An atlantal
725   intercentrum is also present, but has been disarticulated and partially obscures the
726   atlantal centrum.
727   Preserved portions of the axis include the axial centrum and the axial neural arch
728   (Fig. 11A). The anterior end of the axial centrum is shallowly slanted posteriorly, which
729   would have accommodated the axial intercentrum. Ventrally, a small divot is present
730   which which would have contacted the axial intercentrum, indicating that the axial
731   intercentrum would have been positioned underneath the atlantal pleurocentrum as in
732   captorhinids such as *Captorhinus aguti* and *Eocaptorhinus laticeps* (Fox & Bowman,
733   1966; Dilkes & Reisz, 1986). This divot extends as a small ridge to the posterior end of
734   the axial centrum, which results in a pinched ventral surface. The parapophyses are
735   present on the axial centrum but do not extend onto the axial neural arch to the extend
736   observed in *C. aguti* (figure 36 in Fox & Bowman, 1966). Wide, prominent
737   zygapophyses are present on the neural arch, with morphology that closely resembles

738   *C. aguti*. The axial neural spine is tall and possesses an anteroventral projection, as
739   with eureptiles and synapsids. In contrast to the concave posterior base of the axial
740   neural spine in synapsids (Romer & Price, 1940), the neural spine of *Delorhynchus*
741   *cifellii* is smooth.
742   Excluding the atlas-axis complex, a total of four other cervical vertebrae are present
743   in this specimen and are mostly articulated with one another (Fig. 11B-C). This
744   assessment is based partly upon the cervical ribs associated with the specimen, as well
745   as the morphology of the neural spines. While the neural spines of the third and fourth
746   cervicals are posterodorsally directed and approximately one-half the length of the
747   vertebrae, the spines on the fifth and sixth vertebrae are dramatically different in shape.
748   The fifth neural spine is considerably shortened and posteriorly directed, while the sixth
749   neural spine is almost nonexistent and projects anterodorsally. The cervical centra are
750   also strongly pinched in comparison to the dorsals, with the sixth centrum displaying a
751   more intermediate condition. In *Captorhinus* cervicals, based upon personal
752   observation, the third and fourth cervicals display similar pinched texture on their ventral
753   surfaces. However, the fifth and sixth vertebrae, as well as the dorsal vertebrae, do not
754   display this pattern. The prezygapophyses are flattened, dorsally concave and
755   mediolaterally broad. Compared to the prezygapophyses, the postzygapophyses are
756   mediolaterally thinner, dorsally convex and project posteriorly. The zygapophyses as a
757   whole are mediolaterally tilted towards the midline, as is described in *C. aguti* (Fox &
758   Bowman, 1966). Transverse processes are oriented lateroventrally, tapering as they
759   extend anteroventrally. On the fifth and sixth cervicals, a small, rounded pathology
760   protrudes between the zygapophyses on the right side of each vertebra (Fig. 11C), with
761   the pathology on the fifth cervical vertebra being larger than on the sixth.
762   Nineteen dorsal vertebrae are preserved in OMNH 73515, which would result in a
763   minimum count of twenty-five presacral vertebrae (Fig. 11D). It is likely that these
764   vertebrae represent most of the presacral series. In comparison to the cervical
765   vertebrae, the dorsal centra are less pinched. Dorsal neural spines are uniformly one-
766   third the length of the corresponding vertebrae where preserved. The dorsal
767   zygapophyses closely resemble the cervical zygapophyses, with the exceptions of
768   shallower mediolateral tilting and flattened dorsal surfaces. At the posterior end of the
769   prezygapophyses, the dorsal neural arches are sharply pinched inwards. The
770   transverse processes are laterally oriented and proportionately shorter than in the
771   cervical vertebrae.
772   Four cervical ribs are associated with this skeleton, with three from the left side and
773   one on the right (Fig. 1B). The partial articulation of these ribs with cervical vertebrae
774   has led to tentative identification of the fourth left, fifth left and right and sixth left cervical
775   ribs. While the fourth left cervical rib is shortened, triangular and tapers ventrally, the
776   fifth and sixth cervical ribs are relatively elongated and expand ventrally. The dorsal ribs
777   are jumbled together and preserved in varying degrees of completeness, with a total of

778 twenty-five dorsal ends associated with this specimen. Unlike the posterior cervical ribs,
779 the dorsal ribs are ventrally slender and are open at their ventral ends.
780   As with other early Permian reptiles and some synapsids, the paired clavicle consists
781 of a broadened ventral plate overlying the anterior coracoid and interclavicle and a
782 slender dorsal projection that would cap the anterior scapula (Fig. 12A-B). As with
783 *Captorhinus aguti* (Fox & Bowman, 1966; Holmes, 1977), a narrow flange would have
784 slightly enveloped the lateral surface of the scapula, which continues into the ventral
785 plate. Towards the tip of the dorsal projection, a shallow groove runs through the
786 scapular surface which may have marked the suprascapular. The flange extends
787 ventrally and merges into the broad ventral plate, which is notched posteroventrally
788 where it would contact the interclavicle. This flange is thinner than what is observed in
789 *C. aguti* (Fox & Bowman, 1966; Holmes, 1977) and lacks a posterior process.
790   The interclavicle is a T-shaped structure, with a crossbar and stem that most closely
791 resembles the condition in *Milleretta* (Gow, 1972). The ventral portion of the crossbar
792 possesses a thin border projecting anteriorly which would have underlain the clavicle,
793 although the posterolateral section of the border is not inset into the thickened crossbar
794 as in *Captorhinus aguti* (Fox & Bowman, 1966). The medial border is raised slightly,
795 which would have divided the paired clavicles (Fig. 12C-D), as in *Milleretta* (Gow, 1972).
796 Both the dorsal and ventral surfaces of the interclavicle are otherwise smooth. The
797 crossbar and stem of the crossbar are positioned perpendicular to one another as
798 previously described in *Milleretta* (Gow, 1972). This condition contrasts sharply to
799 *Mesosaurus tenuidens*, where the crossbar of the interclavicle gently merges with the
800 stem (Modesto, 2010).
801   The scapulocoracoids are superficially similar to those in eureptiles like *Captorhinus*
802 *aguti*, but with L-shaped plates resembling those of *Mesosaurus tenuidens* (Fox &
803 Bowman, 1966; Holmes, 1977; Modesto, 2010). General morphology can still be
804 described for the scapula and coracoid, but the borders between elements are nearly
805 indistinguishable, with the exception of a shallow suture on the anterior projection of the
806 glenoid fossa (Fig. 12E-F). Whereas the anterior scapula is damaged on both sides, the
807 posterior portion of the scapula is curved anteriorly and comparatively broader than
808 what is described in *C. aguti*. The posterior border of the scapula extends forward
809 slightly resulting in a curved dorsal edge. This condition resembles what is seen in *M.*
810 *tenuidens* (Modesto, 2010), albeit markedly less pronounced. The glenoid buttress
811 resembles the condition of other terrestrial tetrapods but the supraglenoid foramen does
812 not perforate the glenoid buttress. Ventromedially, the coracoid possesses a broad plate
813 extending throughout the entire length of the scapulocoracoid element. The glenoid
814 fossa is the most robust section of the scapulocoracoid, with convex scapular and
815 coracoid projections. Of the two lateral projections in the glenoid fossa, the anterior
816 process is twice as tall as the posterior process and is pierced ventrally by the coracoid
817 foramen. A prominent triceps process arises from the posterior coracoid, extending

818 posterodorsally with a similar length to the posterior projection of the glenoid fossa.
819 Medially, the scapulocoracoid is supported by several ridges as in *C. aguti*, although
820 these ridges expand distally. The coracoid foramen extends anteriorly between the
821 dorsal and anteroventral ridges.
822   The tetraradiate morphology of the humerus found in Permo-Carboniferous tetrapods
823 is shared by *Delorhynchus cifellii* (Fig. 13). The proximal and distal ends of the humerus
824 are twisted at approximate right angles to one another, although the angle is slightly
825 closer to 90° than in *Captorhinus aguti* (Fox & Bowman, 1966). The synapsid condition
826 is remarkably different, where the twist between proximal and distal ends is between
827 35° and 60° (Romer & Price, 1940). On the proximal end of this limb element, the
828 deltopectoral crest projects anteromedially with a shallow dorsal depression. In *C. aguti*,
829 this feature is significantly shorter, and is angled medioventrally with a flattened dorsal
830 surface (Fox & Bowman, 1966). Synapsids such as *Ophiacodon* also possess
831 medioventrally oriented deltopectoral crests, but the angle between the crest and the
832 proximal head is considerably sharper (Romer & Price, 1940). The proximal surface of
833 articulation of the humerus is porous as in *C. aguti* (Fox & Bowman, 1966), but
834 anteriorly the head is shortened and does not extend past the contact with the
835 deltopectoral crest. A broad tuberosity located on the posterior head of the humerus
836 would have supported the latissimus dorsi. Distally, the humerus is broadened and
837 rectangular in shape, as described in *Milleretta* and *Saurodektes* (Gow, 1972; Reisz &
838 Scott, 2002). The entepicondylar foramen is close to the posterior edge of the humerus,
839 with well-defined proximal edges and a sloping distal surface as in *Milleretta* (Gow,
840 1972), although the entepicondylar foramen is positioned further proximally towards the
841 entepicondyle anteriorly. A pronounced ectepicondyle and supinator process are
842 present, as well as an ectepicondylar foramen. This ectepicondylar foramen originates
843 in the groove between the ectepicondyle and supinator process, extends distally
844 through the thickness of the ectepicondyle and opens next to the capitulum. The
845 articulating surface of the humerus also resembles *C. aguti*, but the trochlea is
846 shallower and does not extend as far proximally (Holmes, 1977). In addition, the
847 capitulum is circular as opposed to the proximodistally oriented, oval-shaped capitulum
848 in *C. aguti* (Holmes, 1977).

849

Discussion

851 **Phylogenetic analysis.** The purpose of our phylogenetic analysis is to test the position
852 of *Delorhynchus* among parareptiles using the new anatomical data gleaned from this
853 redescription of the holotype. Information provided by this study greatly enhanced the
854 available cranial data for this pivotal early parareptile, but more importantly also allowed
855 us to add valuable new postcranial data. We therefore updated the latest data matrix
856 (Cisneros et al., 2020) with the new information about *Delorhynchus*, but restricted the
857 analysis to a smaller number of taxa. We felt that there was no need to resort to using

858   the full complement of Paleozoic amniotes and stem amniotes that was previously used
859   and decided to test the relationships of the parareptile *Delorhynchus* within a smaller
860   framework of parareptile evolution and see how our results compare to those of
861   Cisneros et al. (2020). We carefully reevaluated all characters used by previous workers
862   and made some modifications and corrections. All characters were resorted by
863   anatomical position in a format similar to Laurin & Reisz (1995). Three characters were
864   deleted from the analysis and six new characters were added for a total of 193
865   characters. Deleted characters include the presence of dorsal dermal ossifications,
866   number of cusps of marginal dentition and contribution of the squamosal to the lower
867   temporal bar, as these characters were not relevant to the taxa being studied.
868   Characters introduced in this study include an anterolateral shelf of the dorsal process
869   of the maxilla, number of lateral exposures of the lacrimal, texture of the posterior edge
870   of jugal, presence of the quadratojugal dorsal process under the skull roof, stapedial
871   shaft morphology and the contact between the stapedial shaft and the stapedial dorsal
872   process. In this process we also removed some parareptile taxa like *Bashkyroleter* and
873   *Rhipaeosaurus* becausetheir taxonomic identity is somewhat problematic due to
874   consistently paraphyletic results in past studies and incompleteness of material
875   respectively, and because their position among the 'nycteroleters' is unresolved (Tsuji et
876   al., 2012). In addition, we also removed the so-called 'parareptile' *Carbonodraco* from
877   this analysis because we are not convinced that it is a parareptile, as reported in Mann
878   et al. (2019), and we believe that its limited remains require further study.
879   **Results of analysis.** The strict consensus of 2 most parsimonious cladograms of
880   parareptile relationships is shown in Figure 14. The data indicates that this is a weakly
881   supported tree topology, but at the same time the results of our analysis confirm the
882   status of *Delorhynchus* as a sister taxon to *Colobomycter*, within a clade that includes
883   the known acleistorhinids. However the overall composition of the 'acleistorhinids' has a
884   somewhat novel topology, with the larger clade that includes *Feeserpeton*,
885   *Lanthanosuchus* and *Acleistorhinus* being successive outgroups to the clade comprising
886   *Karutia*, *Delorhynchus* and *Colobomycter*. Perhaps most surprisingly, this clade of
887   'acleistorhinids' is the sister taxon to the other major clade of early parareptiles, the
888   bolosaurids. This pattern is contrary to previous analyses which have placed
889   bolosaurids in a more basal position among parareptiles, between the Gondwanan
890   *Milleretta* and *Australothyris* (Cisneros et al., 2020). The interesting position of the
891   Gondwanan *Milleretta* and *Australothyris* at the base of parareptiles also recovered
892   previously (Cisneros et al., 2020) raises some interesting questions regarding the
893   geographic origin and patterns of dispersal of parareptiles, especially in view of the
894   undisputed fact that the oldest parareptiles are restricted to Laurasia.
895   There are some other notable differences between our results and those of previous
896   studies. Interestingly, and not entirely unexpectedly, *Mesosaurus* becomes a sister
897   taxon to the clade normally considered to be Eureptilia. The position of *Mesosaurus*

898 among either parareptiles (Modesto, 2006; Cisneros et al., 2020) or among eureptiles
899 (Modesto et al., 2015; Laurin & Piñeiro, 2017) is weakly supported and we suggest that
900 this is because much of the anatomical evidence that could help evaluate the
901 phylogenetic relationships of this taxon has been 'overprinted' by numerous
902 autapomorphies.
903   The anatomy of the mysterious *Lanthanosuchus* and its closest relatives has always
904 been somewhat controversial, again a taxon possessing a large number of
905 autapomorphies and little-known postcranial anatomy. The most recent parareptile
906 phylogeny (Cisneros et al., 2020) posited that *Lanthanosuchus* is a sister taxon to the
907 'nycteroleters'. Instead, our results place this taxon as a sister to *Acleistorhinus*, as
908 previously suggested (MacDougall et al., 2017b). We use the term 'acleistorhinids' in an
909 informal manner because the clade now includes not only the usual suspects as shown
910 in the most recent phylogenetic analysis (Cisneros et al., 2020), but also includes
911 *Lanthanosuchus*.
912   Bootstrap values indicate that the position of *Mesosaurus* as a eureptile is weak, and
913 clearly needs reevaluation. For example, the evidence for the presence of a lateral
914 temporal fenestra is controversial (Modesto, 2006; Laurin & Piñeiro, 2017), as is the
915 homology of the "swelling" of the vertebral neural arches. Furthermore, critical aspects
916 of the braincase of the highly autapomorphic mesosaurs are missing, making their
917 overall detailed anatomical reexamination worthwhile. Among 'acleistorhinids', only the
918 bootstrap values for the clade of *Delorhynchus* and *Colobomycter* is high. We interpret
919 the low values for the overall clade on a combination of factors, one being the very
920 fragmentary nature of *Karutia* and the other being the lack of data on the postcranial
921 anatomy of *Lanthanosuchus* and *Acleistorhinus*.
922

Conclusions

924 These results indicate that much work still needs to be undertaken for a better
925 understanding of the initial stages of parareptile evolution, and hopefully new, more
926 completely preserved fossil material like those described in this study will be uncovered.
927 We refrained from considering the relationships of parareptiles with other amniote
928 clades, as such a task is well beyond the objectives of this study. However, this new
929 data together with emerging new information on other parareptiles and synapsids will
930 provide the impetus for re-evaluating the position of 'acleistorhinids' and other
931 parareptiles among amniotes.
932

Acknowledgements

934 We would like to thank Mr. W. J. May for his many years of generous contribution of Dolese
935 material, and the staff of the Oklahoma Museum of Natural History for the loan of this specimen.
936 We would also like to thank Ms. D. M. Scott in preparation and general assistance with
937 anatomy.

938

References

940 Bazzana KD, Evans DC, Bevitt JJ, Reisz RR. 2021. Neurosensory anatomy of
941 Varanopidae and its implications for early synapsid evolution. Journal of Anatomy
942 240:833–849. DOI: 10.1111/joa.13593.
943 Berman DS. 2000. Early Permian bipedal reptile. Science 290:969-972. DOI
944 10.1126/science.290.5493.969
945 Berman DS, Maddin HC, Henrici AC, Sumida SS, Scott D, Reisz RR. 2020. New
946 Primitive Caseid (Synapsida, Caseasauria) from the Early Permian of Germany. Annals
947 of Carnegie Museum 86:43–75. DOI: 10.2992/007.086.0103.
948 Berman DS, Reisz RR, Scott D, Henrici AC, Sumida SS, Martens T. 2000. Early
949 Permian bipedal reptile. Science 290:969–972. DOI: 10.1126/science.290.5493.969.
950 Carroll RL, Lindsay W. 1985. Cranial anatomy of the primitive reptile *Procolophon*.
951 Canadian Journal of Earth Sciences 22:1571–1587.
952 Cisneros JC, Kammerer CF, Angielczyk KD, Fröbisch J, Marsicano C, Smith RMH,
953 Richter M. 2020. A new reptile from the lower Permian of Brazil (*Karutia fortunata* gen.
954 et sp. nov.) and the interrelationships of Parareptilia. Journal of Systematic
955 Palaeontology 18:1939–1959. DOI: 10.1080/14772019.2020.1863487.
956 Daly E. 1969. A New Procolophonoid Reptile from the Lower Permian of Oklahoma.
957 Source: Journal of Paleontology 43:676–687.
958 deBraga M, Reisz RR. 1996. The early permian reptile *Acleistorhinus pteroticus* and its
959 phylogenetic position. Journal of Vertebrate Paleontology 16:384–395. DOI:
960 10.1080/02724634.1996.10011328.
961 Dilkes DW, Reisz RR. 1986. The axial skeleton of the Early Permian reptile
962 *Eocaptorhinus laticeps* (Williston). Earth Sci 23:1288–1296.
963 Fox RC. 1962. Two new pelycosaurs from the Lower Permian of Oklahoma. University
964 of Kansas Publications, Museum of Natural History 12:297–307.
965 Fox RC, Bowman MC. 1966. Osteology and relationships of *Captorhinus aguti* (Cope)
966 (Reptilia: Captorhinomorpha). The University of Kansas Paleontological
967 Contributions:1–79.
968 Garbe U, Randall T, Hughes C, Davidson G, Pangelis S, Kennedy SJ. 2015. A New
969 Neutron Radiography / Tomography / Imaging Station DINGO at OPAL. In: Physics
970 Procedia. Elsevier B.V., 27–32. DOI: 10.1016/j.phpro.2015.07.003.
971 Gow CE. 1972. The osteology and relationships of the Millerettidae (Reptilia:
972 Cotylosauria). J. Zool 167:219–264.
973 Haridy Y, Macdougall MJ, Reisz RR. 2018. The lower jaw of the Early Permian
974 parareptile *Delorhynchus*, first evidence of multiple denticulate coronoids in a reptile.
975 Zoological Journal of the Linnean Society 184:791–803. DOI:
976 10.1093/zoolinnean/zlx085.

977   Haridy Y, Macdougall MJ, Scott D, Reisz RR. 2016. Ontogenetic Change in the
978   Temporal Region of the Early Permian Parareptile *Delorhynchus cifellii* and the
979   Implications for Closure of the Temporal Fenestra in Amniotes. PLoS ONE
980   11:e0166819. DOI: 10.1371/journal.pone.0166819.
981   Heaton M. 1979. Cranial anatomy of primitive captorhinid reptiles from the late
982   Pennsylvanian and Early Permian Oklahoma and Texas. In: Oklahoma Geological
983   Survey. 1–81.
984   Holmes R. 1977. The Osteology and Musculature of the Pectoral Limb of Small
985   Captorhinids. Journal of Morphology 152:101–140.
986   Laurin M, Piñeiro GH. 2017. A reassessment of the taxonomic position of mesosaurs,
987   and a surprising phylogeny of early amniotes. Frontiers in Earth Science 5. DOI:
988   10.3389/feart.2017.00088.
989   MacDougall MJ, Brocklehurst N, Fröbisch J. 2019. Species richness and disparity of
990   parareptiles across the end-Permian mass extinction. Proceedings. Biological sciences
991   286:20182572. DOI: 10.1098/rspb.2018.2572.
992   MacDougall MJ, Modesto SP, Reisz RR. 2016. A new reptile from the Richards Spur
993   locality, Oklahoma, U.S.A., and patterns of Early Permian parareptile diversification.
994   Journal of Vertebrate Paleontology 36:e1179641. DOI:
995   10.1080/02724634.2016.1179641.
996   MacDougall MJ, Reisz RR. 2012. A new parareptile (Parareptilia, Lanthanosuchoidea)
997   from the Early Permian of Oklahoma. Journal of Vertebrate Paleontology 32:1018–
998   1026. DOI: 10.1080/02724634.2012.679757.
999   MacDougall MJ, Reisz RR. 2014. The first record of a nyctiphruretid parareptile from the
1000   Early Permian of North America, with a discussion of parareptilian temporal
1001   fenestration. Zoological Journal of the Linnean Society 172:616–630. DOI:
1002   10.1111/zoj12180.
1003   MacDougall MJ, Scott D, Modesto SP, Williams SA, Reisz RR. 2017. New material of
1004   the reptile *Colobomycter pholeter* (Parareptilia: Lanthanosuchoidea) and the diversity of
1005   reptiles during the Early Permian (Cisuralian). Zoological Journal of the Linnean Society
1006   180:661–671.
1007   MacDougall MJ, Tabor NJ, Woodhead J, Daoust AR, Reisz RR. 2017. The unique
1008   preservational environment of the Early Permian (Cisuralian) fossiliferous cave deposits
1009   of the Richards Spur locality, Oklahoma. Palaeogeography, Palaeoclimatology,
1010   Palaeoecology 475:1–11. DOI: 10.1016/j.palaeo.2017.02.019.
1011   Mann A, McDaniel EJ, McColville ER, Maddin HC. 2019. *Carbonodraco lundi* gen et sp.
1012   Nov., the oldest parareptile, from Linton, Ohio, and new insights into the early radiation
1013   of reptiles. Royal Society Open Science 6. DOI: 10.1098/rsos.191191.
1014   Mays C, Bevitt J, Stillwell J. 2017. Pushing the limits of neutron tomography in
1015   paleontology: Three-dimensional modelling of in-situ resin within fossil plants.
1016   Paleontologica Electronica 20.3(57A):1-12

1017   Modesto SP. 1999. *Colobomycter pholeter* from the Lower Permian of Oklahoma: a
1018   parareptile, not a protorothyridid. Journal of Vertebrate Paleontology 19:466–472. DOI:
1019   10.1080/02724634.1999.10011159.
1020   Modesto SP. 2006. The cranial skeleton of the Early Permian aquatic reptile
1021   *Mesosaurus tenuidens*: implications for relationships and palaeobiology. Zoological
1022   Journal of the Linnean Society 146:345–368. DOI: 10.1111/j.1096-3642.2006.00205.x.
1023   Modesto SP. 2010. The postcranial skeleton of the aquatic parareptile *Mesosaurus*
1024   *tenuidens* from the Gondwanan Permian. Journal of Vertebrate Paleontology 30:1378–
1025   1395. DOI: 10.1080/02724634.2010.501443.
1026   Modesto SP, Reisz RR. 2008. New material of *Colobomycter pholeter*, a small
1027   parareptile from the Lower Permian of Oklahoma. Journal of Vertebrate Paleontology
1028   28:677–684. DOI: 10.1671/0272-4634(2008)28[677:NMOCPA]2.0.CO;2.
1029   Modesto SP, Scott DM, Macdougall MJ, Sues H-D, Evans DC, Reisz RR. 2015. The
1030   oldest parareptile and the early diversification of reptiles. Proceedings. B 282. DOI:
1031   10.1098/rspb.2014.1912.
1032   Modesto SP, Scott DM, Reisz RR. 2009. Arthropod remains in the oral cavities of fossil
1033   reptiles support inference of early insectivory. Biology Letters 5:838–840. DOI:
1034   10.1098/rsbl.2009.0326.
1035   Müller J, Li J-L, Reisz RR. 2008. A new bolosaurid, Belebey chengi sp. nov., from the
1036   Middle Permian of China and its paleogeographic significance. Naturwissenschaften
1037   95:1169-1174. DOI 10.1007/s00114-008-0438-0.
1038   Olson, E. C. (1947). The family Diadectidae and its bearing on the classification of
1039   reptiles. Fieldiana (Geology) 11:1-53.
1040   Reisz RR, Barkas V, Scott D. 2002. A new early Permian bolosaurid reptile from the
1041   Richards Spur Dolese Brothers Quarry, near Fort Sill, Oklahoma. Journal of Vertebrate
1042   Paleontology 22:23–28. DOI: 10.1671/0272-4634(2002)022[0023:ANEPBR]2.0.CO;2.
1043   Reisz RR, Berman DS. 2001. The skull of *Mesenosaurus romeri*, a small varanopseid
1044   (Synapsida: Eupelycosauria) from the Upper Permian of the Mezen River Basin,
1045   Northern Russia. Annals of Carnegie Museum 70:113–132.
1046   Reisz R, Haridy Y, Müller J. 2016. *Euconcordia* nom. nov., a replacement name for the
1047   captorhinid eureptile Concordia Müller and Reisz, 2005 (non Kingsley, 1880), with new
1048   data on its dentition. Vertebrate Anatomy Morphology Palaeontology 3. DOI:
1049   10.18435/b53w22.
1050   Reisz RR, Macdougall MJ, Modesto SP. 2014. A new species of the parareptile genus
1051   *Delorhynchus*, based on articulated skeletal remains from Richards Spur, Lower
1052   Permian of Oklahoma. Journal of Vertebrate Paleontology 34:1033–1043.
1053   Reisz RR, Müller J, Tsuji L, Scott D. 2007. The cranial osteology of *Belebey vegrandis*
1054   (Parareptilia: Bolosauridae), from the Middle Permian of Russia, and its bearing on
1055   reptilian evolution. Zoological Journal of the Linnean Society 151:191–214. DOI:
1056   10.1111/j.1096-3642.2007.00312.x.

1057 Reisz RR, Scott D. 2002. *Owenetta kitchingorum*, sp. nov., a small parareptile
1058 (Procolophonia: Owenettidae) from the Lower Triassic of South Africa. Journal of
1059 Vertebrate Paleontology 22:244–256. DOI: 10.1671/0272-
1060 4634(2002)022[0244:OKSNAS]2.0.CO;2.
1061 Romer AS, Price LW. 1940. Review of the Pelycosauria. 28:1–538.
1062 Rowe DCT, Scott DM, Bevitt JJ, Reisz RR. 2021. Multiple Tooth-Rowed Parareptile
1063 From the Early Permian of Oklahoma. Frontiers in Earth Science 9:1–11. DOI:
1064 10.3389/feart.2021.709497.
1065 Tsuji LA. 2006. Cranial anatomy and phylogenetic affinities of the Permian parareptile
1066 Macroleter poezicus. Journal of Vertebrate Paleontology 26:849–865. DOI:
1067 10.1671/0272-4634(2006)26[849:CAAPAO]2.0.CO;2.
1068 Tsuji LA, Müller J. 2009. Assembling the history of the Parareptilia: Phylogeny,
1069 diversification, and a new definition of the clade. Fossil Record 12:71–81. DOI:
1070 10.1002/mmng.200800011.
1071 Tsuji LA, Müller J, Reisz RR. 2010. *Microleter mckinzieorum* gen. et sp. nov. from the
1072 Lower Permian of Oklahoma: the basalmost parareptile from Laurasia. Journal of
1073 Systematic Palaeontology 8:245–255. DOI: 10.1080/14772010903461099.
1074 Tsuji LA, Müller J, Reisz RR. 2012. Anatomy of Emeroleter levis and the phylogeny of
1075 the nycteroleter parareptiles. Journal of Vertebrate Paleontology 32:1, 45-67. DOI:
1076 10.1080/02724634.2012.626004.
1077 Vaughn PP. 1958. On a New Pelycosaur from the Lower Permian of Oklahoma, and on
1078 the Origin of the Family Caseidae. Journal of Paleontology 32:981–991.

1079
1080 **Figure 1: Holotype of *Delorhynchus cifellii*, OMNH 73515**. (A) Dorsal view and (B) ventral views.
1081 Abbreviations: sg = shoulder girdle, vc = vertebral column.

1082 **Figure 2: Cranial material of *Delorhynchus cifellii*, OMNH 73515**. (A) Dorsal, (B) lateral and (C) ventral
1083 views. Abbreviations: an = angular, art = articular, bh = basihyal, bo = basioccipital, ch = ceratohyal, cr2 =
1084 second coronoid ossification, d = dentary, ect = ectopterygoid, epi = epipterygoid, f = frontal, j = jugal, la =
1085 lacrimal, m = maxilla, n = nasal, nc = neurocranium, p = parietal, pal = palatine, pbs = parabasisphenoid,
1086 pf = postfrontal, po = postorbital, pp = postparietal, prf = prefrontal, pt = pterygoid, q = quadrate, qj =
1087 quadratojugal, s = stapes, sm = septomaxilla sp = splenial, sph = sphenethmoid, sq = squamosal, st =
1088 supratemporal, v = vomer.
1089
1090 **Figure 3: Right maxilla of Delorhynchus cifellii, OMNH 73515**. (A) Lateral and (B) medial views.
1091
1092 **Figure 4: Internal view of skull roof of *Delorhynchus cifellii*, OMNH 73515**. (A) Ventral view of skull
1093 roof and (B) medial view of right skull roof. Abbreviations: f = frontal, j = jugal, m = maxilla, n = nasal, p =
1094 parietal, pf = postfrontal, po = postorbital, pp = postparietal, prf = prefrontal, qj = quadratojugal, sm =
1095 septomaxilla, sq = squamosal, st = supratemporal, t = tabular.
1096
1097 **Figure 5: Palate and braincase of *Delorhynchus cifellii*, OMNH 73515.** (A) Dorsal, (B) lateral and (C)
1098 ventral views. bh = basihyal, bo = basioccipital, ch = ceratohyal, ect = ectopterygoid, epi = epipterygoid,

1099   ex = exoccipital, nc = neurocranium, pal = palatine, pbs = parabasisphenoid, pt = pterygoid, q = quadrate,
1100   s = stapes, sph = sphenethmoid, v = vomer.

1101

1102   **Figure 6: Parabasisphenoid and sphenethmoid of Delorhynchus cifellii**, **OMNH 73515**. (A) Dorsal,
1103   (B) lateral and (C) ventral views. Abbreviations: bpt. tub. = basipterygoid tuberosity, cult. pr. = cultriform
1104   process, d. pr. = dorsal process of sphenethmoid, d.s. = dorsum sellae, pbs = parabasisphenoid, pr. sell.
1105   = processus sellaris, sph = sphenethmoid, v. k. = ventral keel, vid. sul. = vidian sulcus.

1106

1107   **Figure 7: Right stapes of *Delorhynchus cifellii,* OMNH 73515**. (A) Anterior, (B) dorsal and (C) occipital
1108   views. Abbreviations: d. pr. = dorsal process of stapes, fp = footplate, s. for. = stapedial foramen, s. sh. =
1109   stapedial shaft.

1110

1111   **Figure 8: Supraoccipital-prootic-opisthotic complex of Delorhynchus cifellii, OMNH 73515**. (A)
1112   Anterior, (B) dorsal and (C) occipital views. Abbreviations: op = opisthotic, par = paroccipital processes of
1113   opisthotic, pro = prootic, sup = supraoccipital, ven = venous notches.

1114

1115   **Figure 9: Semicircular canals of *Delorhynchus cifellii,* OMNH 73515**. (A) Anterior view, (B) lateral
1116   view and (C) occipital view of neurocranium, (D) anterior view, (E) lateral view, (F) dorsal view and (G)
1117   occipital view of left semicircular canals. Abbreviations: aasc = ampulla of anterior semicircular canal, alsc
1118   = ampulla of lateral semicircular canal, asc = anterior semicircular canal, cc = common crus, lsc = lateral
1119   semicircular canal, op = opisthotic, par = paroccipital process of opisthotic, pro = prootic, psc = posterior
1120   semicircular canal, sup = supraoccipital, vs = vestibule.

1121

1122   **Figure 10: Mandible of *Delorhynchus cifellii,* OMNH 73515.** (A) Dorsal view of mandible, (B) medial
1123   view of right mandible and (C) lateral view of right mandible. Abbreviations: an = angular, art = articular,
1124   cr1 = first coronoid ossification, cr2 = second coronoid ossification, d = dentary, p. Mck. f. = posterior
1125   Meckelian fossa, pra = prearticular, sur = surangular.

1126

1127   **Figure 11: Representative vertebrae of *Delorhynchus cifellii,* OMNH 73515 in anterior, lateral,**
1128   **dorsal, and ventral views.** (A) Axis vertebra, (B) third cervical vertebra, (C) sixth cervical vertebra and
1129   (D) anterior dorsal vertebra.

1130

1131   **Figure 12: Shoulder girdle elements of *Delorhynchus cifellii,* OMNH 73515.** (A) Lateral view and (B)
1132   medial view of left clavicle, (C) dorsal and (D) ventral views of interclavicle, (E) lateral view and (F) medial
1133   view of left scapulocoracoid. Abbreviations: gl = glenoid, gl. for. = glenoid foramen, sg. for. = supraglenoid
1134   foramen.

1135

1136   **Figure 13: Left humerus of OMNH 73515**. (A) Proximal dorsal, (B) proximal ventral, (C) distal dorsal, (D)
1137   distal ventral, (E) proximal end and (F) distal views. Abbreviations: cap = capitulum, dpc = deltopectoral
1138   crest, ectp = ectepicondyle, ectp. for. = ectepicondylar foramen, entp = entepicondyle, entp. for. =
1139   entepicondylar foramen, l. dor. att. = attachment point of latissimus dorsi, sup. pr. = supinator process, tro
1140   = trochlea.

1141

1142   **Figure 14: Strict consensus of 2 most parsimonious cladograms of parareptile relationships**
1143   **(length 878 steps).** Bootstrap values (>50%) have been provided before the nodes.

Figure 1

Holotype of *Delorhynchus cifellii*, OMNH 73515.

(A) Dorsal view and (B) ventral views. Abbreviations: sg = shoulder girdle, vc = vertebral column.

Figure 2

Cranial material of *Delorhynchus cifellii,* OMNH 73515.

(A) Dorsal, (B) lateral and (C) ventral views. Abbreviations: an = angular, art = articular, bh = basihyal, bo = basioccipital, ch = ceratohyal, cr2 = second coronoid ossification, d = dentary, ect = ectopterygoid, epi = epipterygoid, f = frontal, j = jugal, la = lacrimal, m = maxilla, n = nasal, nc = neurocranium, p = parietal, pal = palatine, pbs = parabasisphenoid, pf = postfrontal, po = postorbital, pp = postparietal, prf = prefrontal, pt = pterygoid, q = quadrate, qj = quadratojugal, s = stapes, sm = septomaxilla sp = splenial, sph = sphenethmoid, sq = squamosal, st = supratemporal, v = vomer.
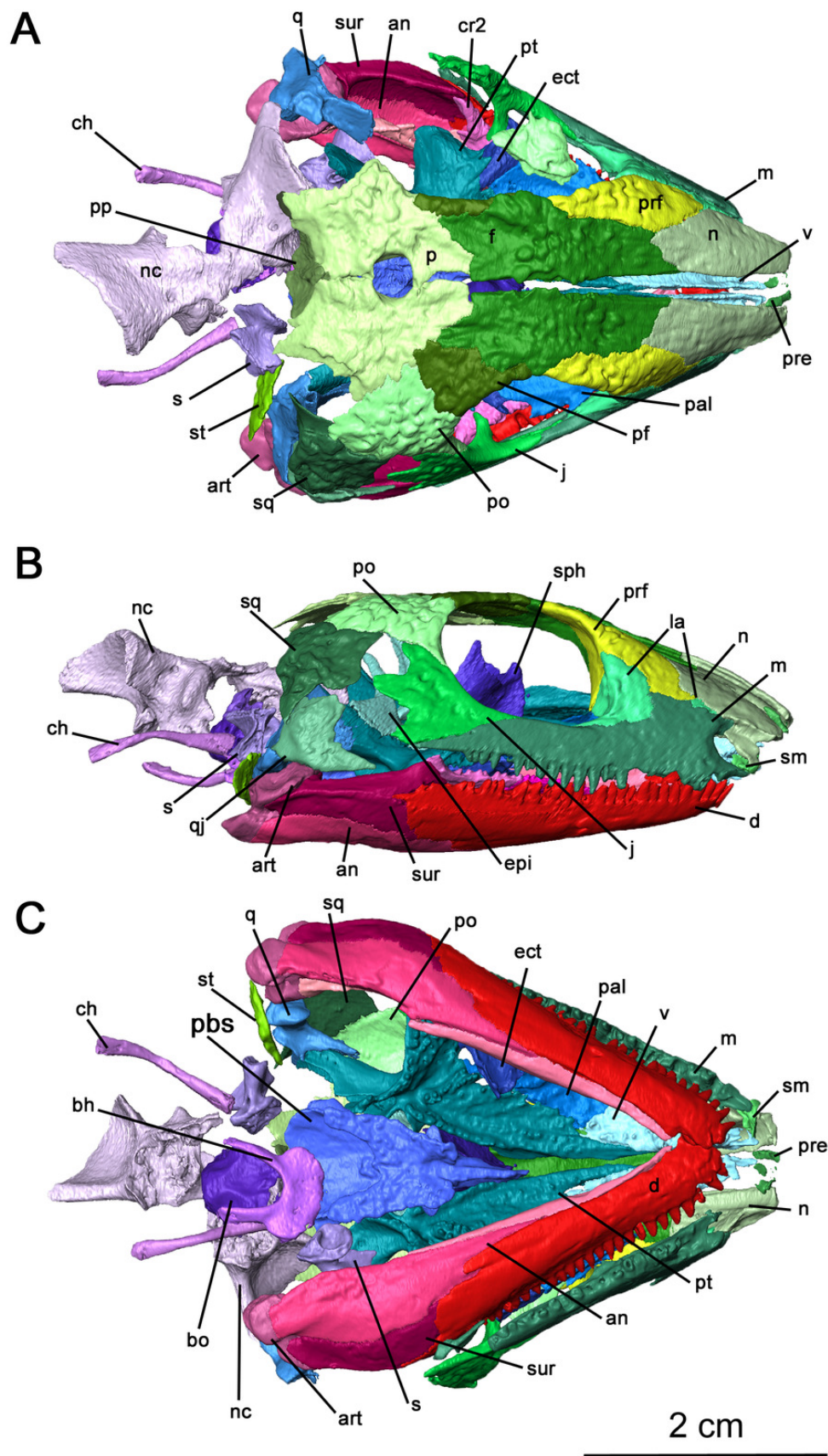
Figure 3

Right maxilla of *Delorhynchus cifellii*, OMNH 73515.
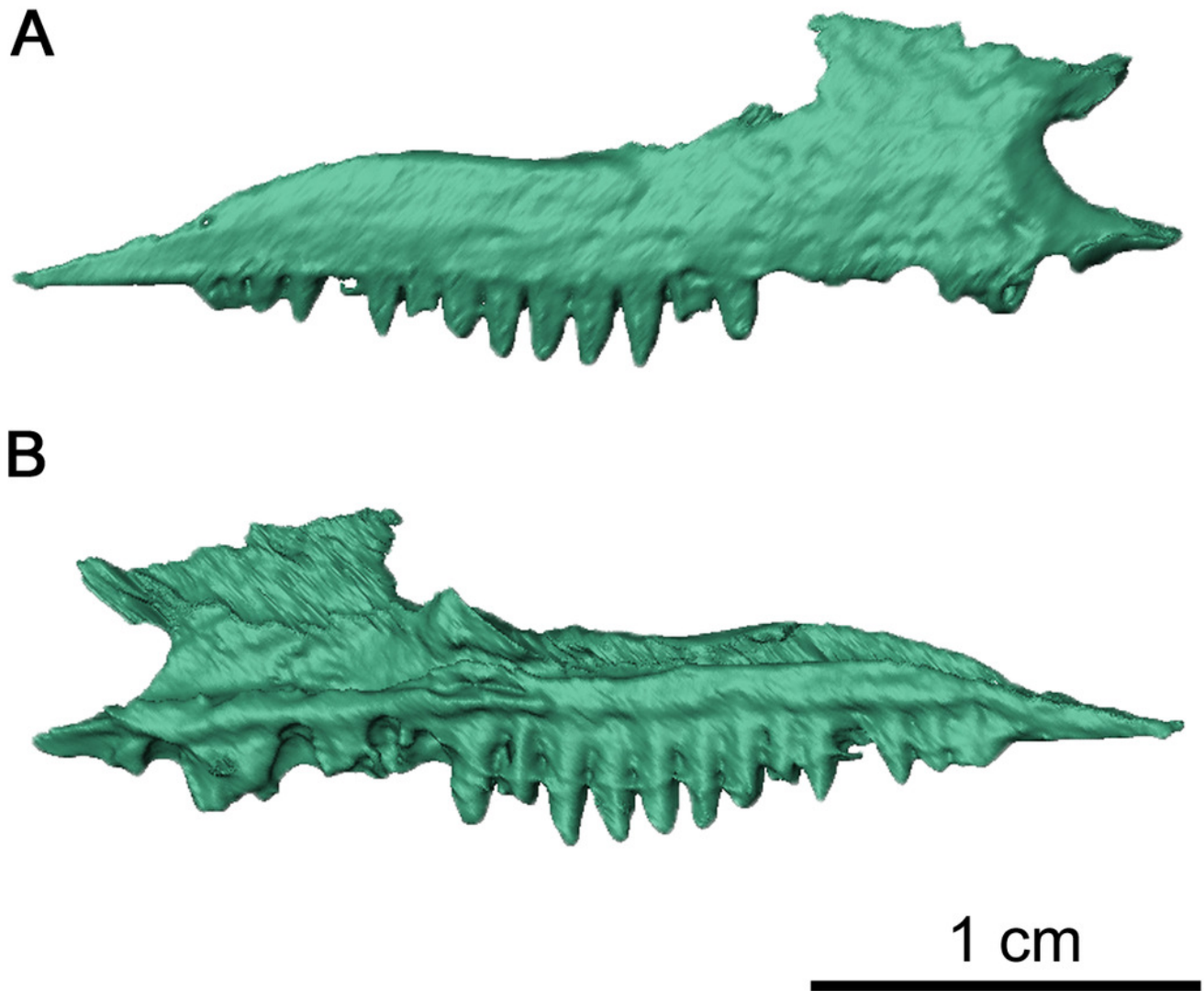
(A) Lateral and (B) medial views.

1 cm

Figure 4

Internal view of skull roof of *Delorhynchus cifellii*, OMNH 73515.

(A) Ventral view of skull roof and (B) medial view of right skull roof. Abbreviations: f = frontal, j = jugal, m = maxilla, n = nasal, p = parietal, pf = postfrontal, po = postorbital, pp = postparietal, prf = prefrontal, qj = quadratojugal, sm = septomaxilla, sq = squamosal, st = supratemporal, t = tabular.
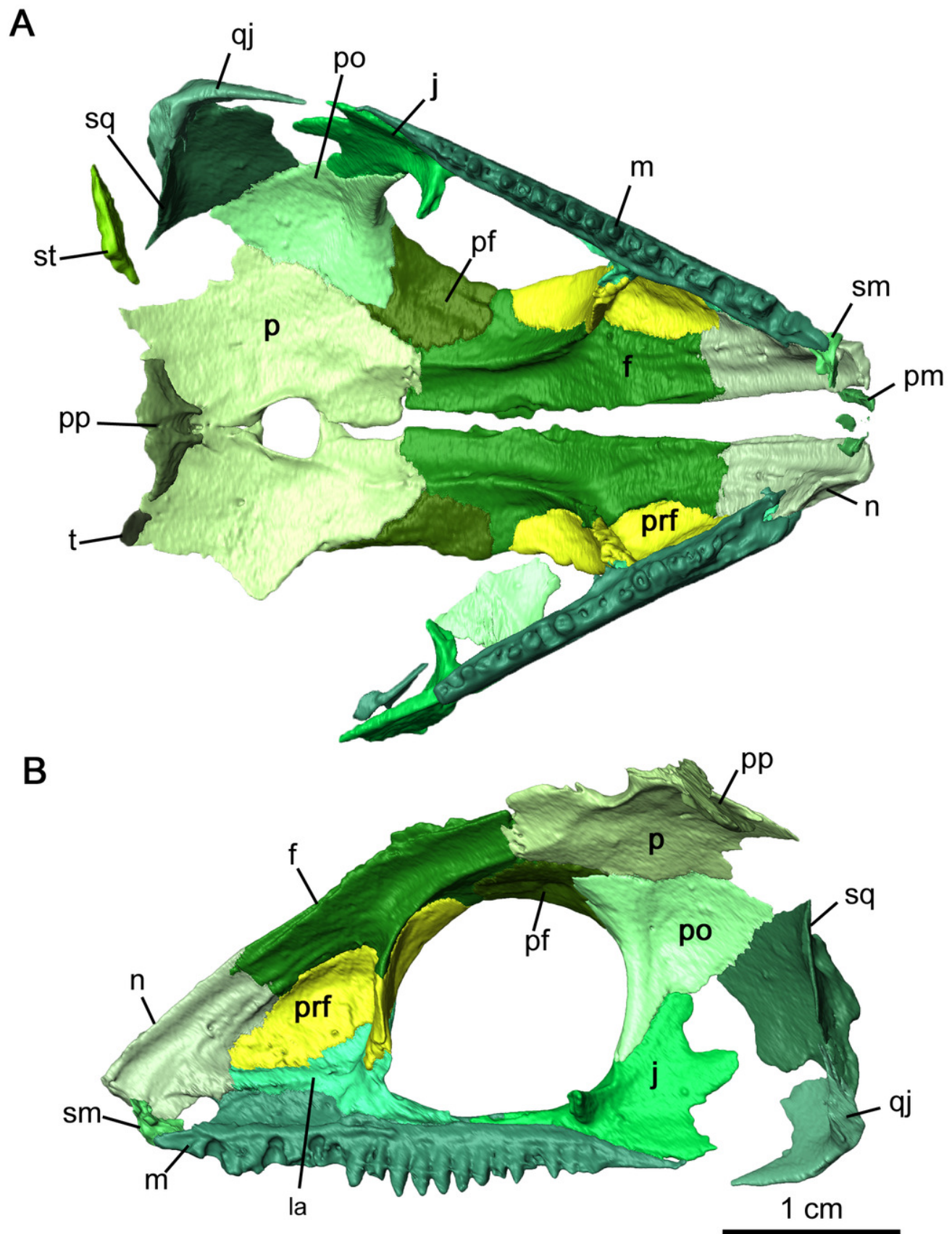
Figure 5

Palate and braincase of *Delorhynchus cifellii,* OMNH 73515.

(A) Dorsal, (B) lateral and (C) ventral views. bh = basihyal, bo = basioccipital, ch = ceratohyal, ect = ectopterygoid, epi = epipterygoid, ex = exoccipital, nc = neurocranium, pal = palatine, pbs = parabasisphenoid, pt = pterygoid, q = quadrate, s = stapes, sph = sphenethmoid, v = vomer.
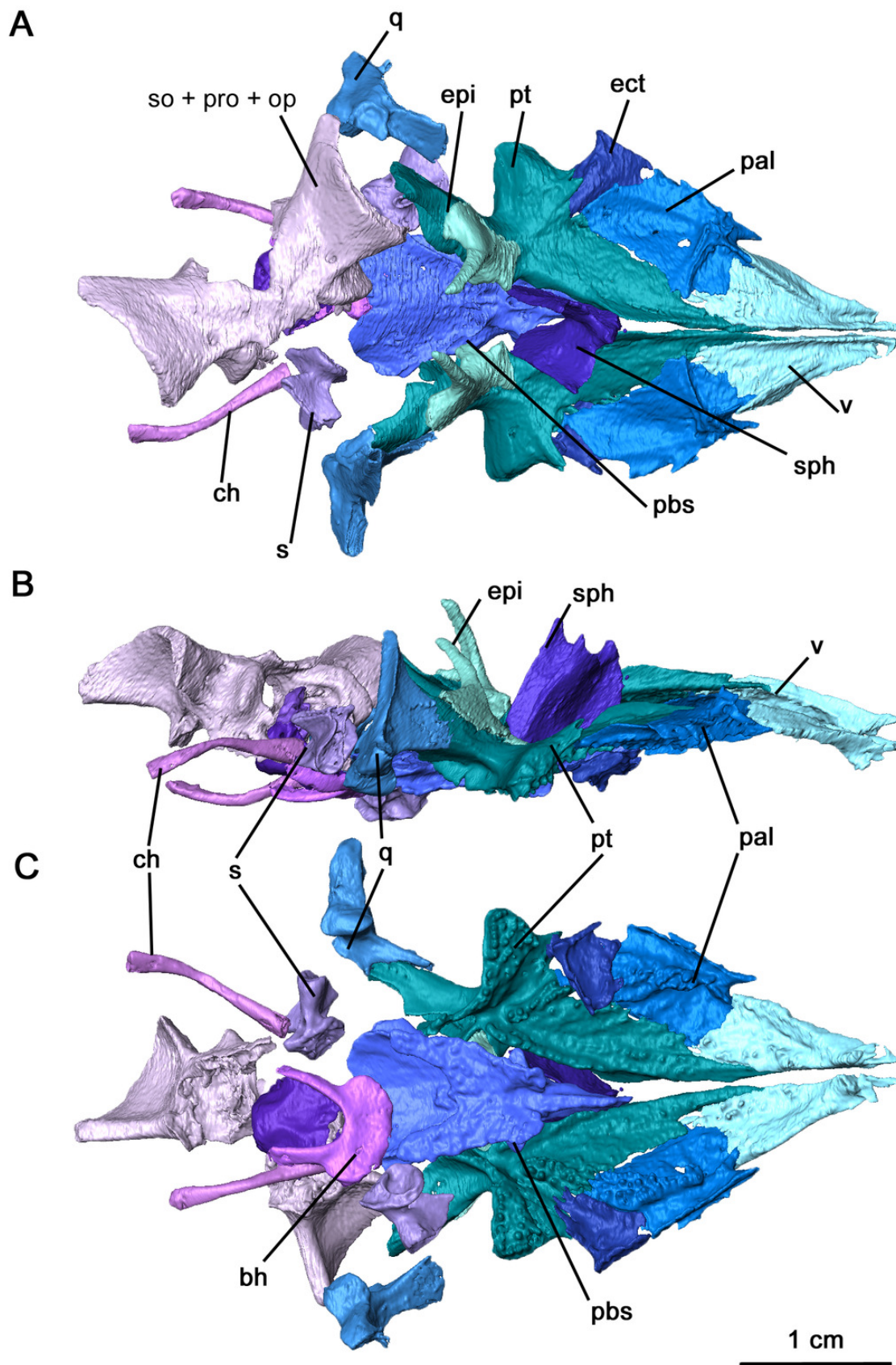
Figure 6

Parabasisphenoid and sphenethmoid of *Delorhynchus cifellii*, OMNH 73515.

(A) Dorsal, (B) lateral and (C) ventral views. Abbreviations: bpt. tub. = basipterygoid tuberosity, cult. pr. = cultriform process, d. pr. = dorsal process of sphenethmoid, d.s. = dorsum sellae, pbs = parabasisphenoid, pr. sell. = processus sellaris, sph = sphenethmoid, v. k. = ventral keel, vid. sul. = vidian sulcus.
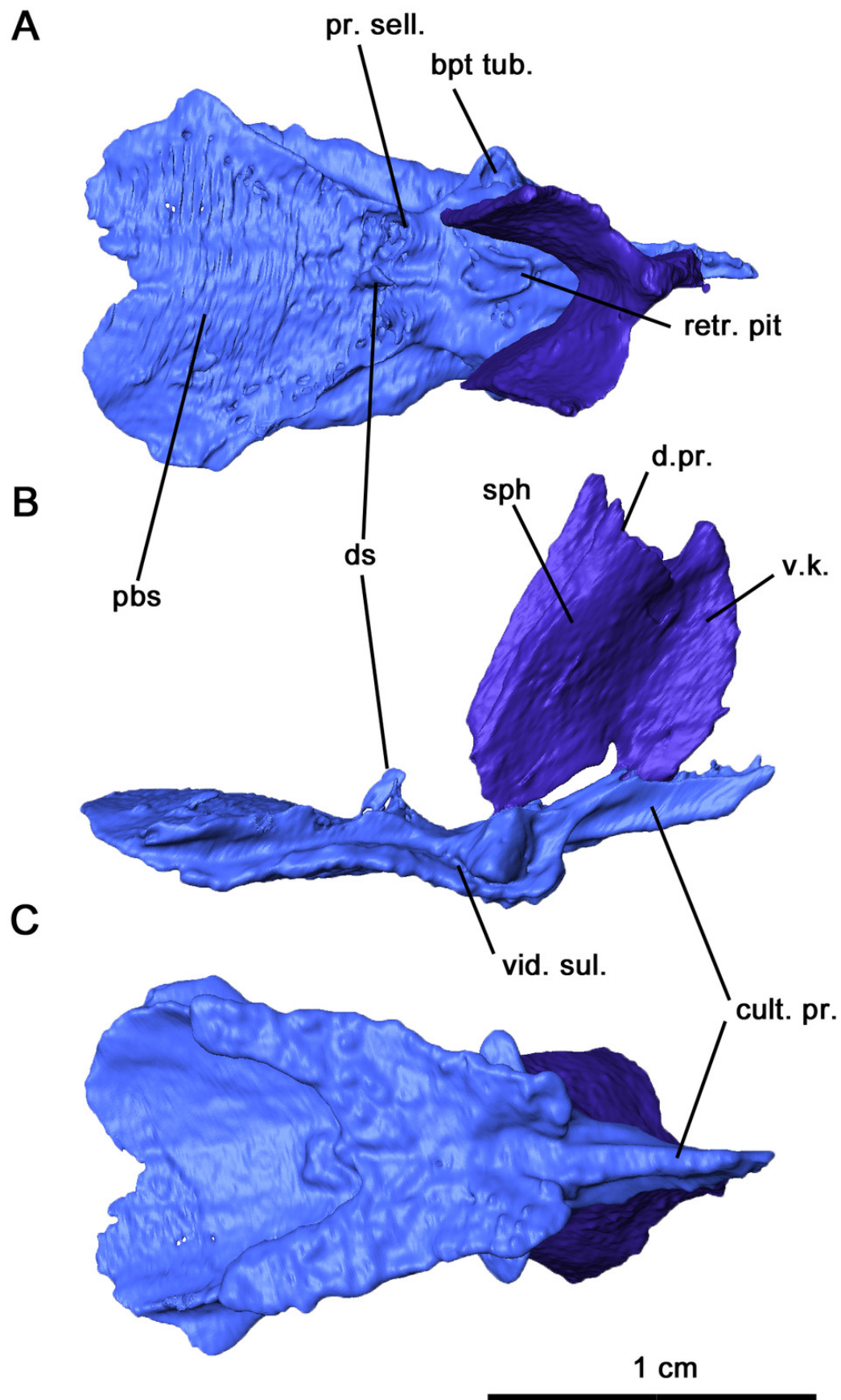
Figure 7

Right stapes of *Delorhynchus cifellii,* OMNH 73515.

(A) Anterior, (B) dorsal and (C) occipital views. Abbreviations: d. pr. = dorsal process of stapes, fp = footplate, s. for. = stapedial foramen, s. sh. = stapedial shaft.
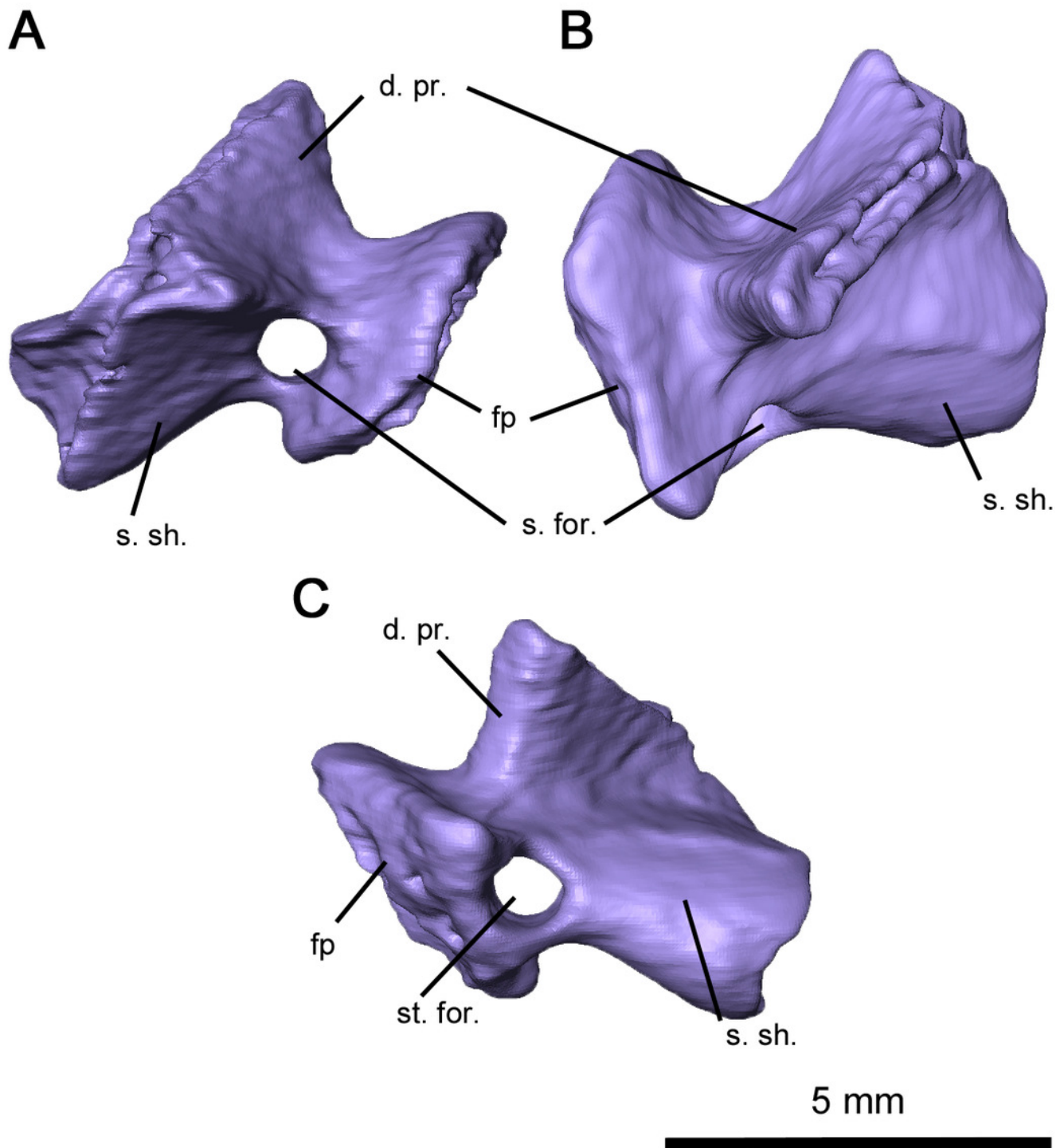
Figure 8

Supraoccipital-prootic-opisthotic complex of *Delorhynchus cifellii*, OMNH 73515.

(A) Anterior, (B) dorsal and (C) occipital views. Abbreviations: op = opisthotic, par = paroccipital processes of opisthotic, pro = prootic, sup = supraoccipital, ven = venous notches.
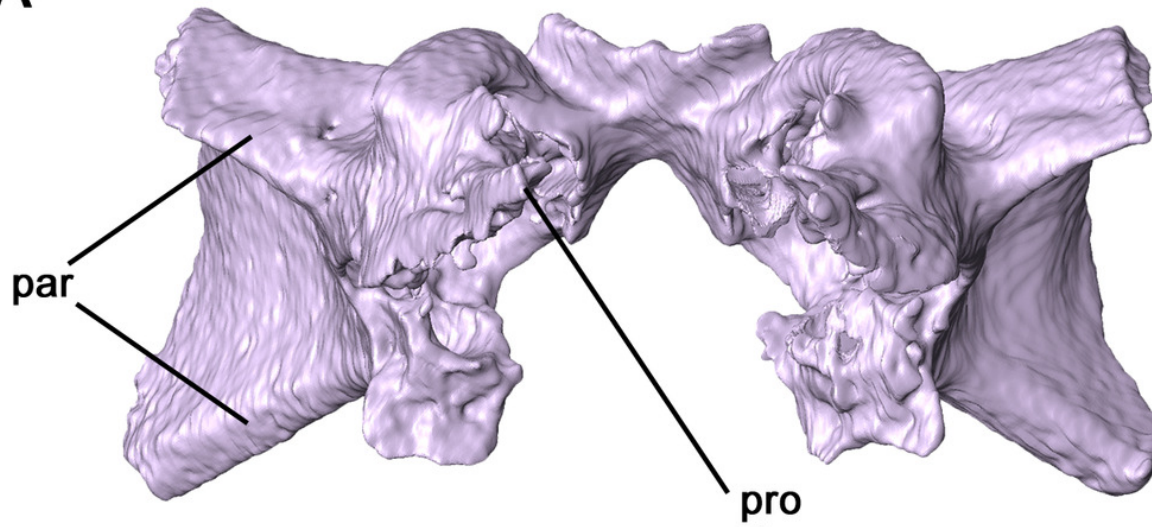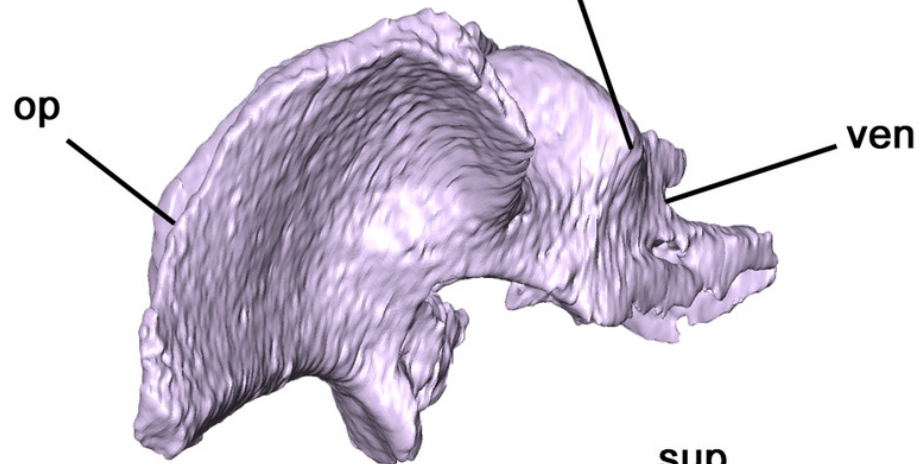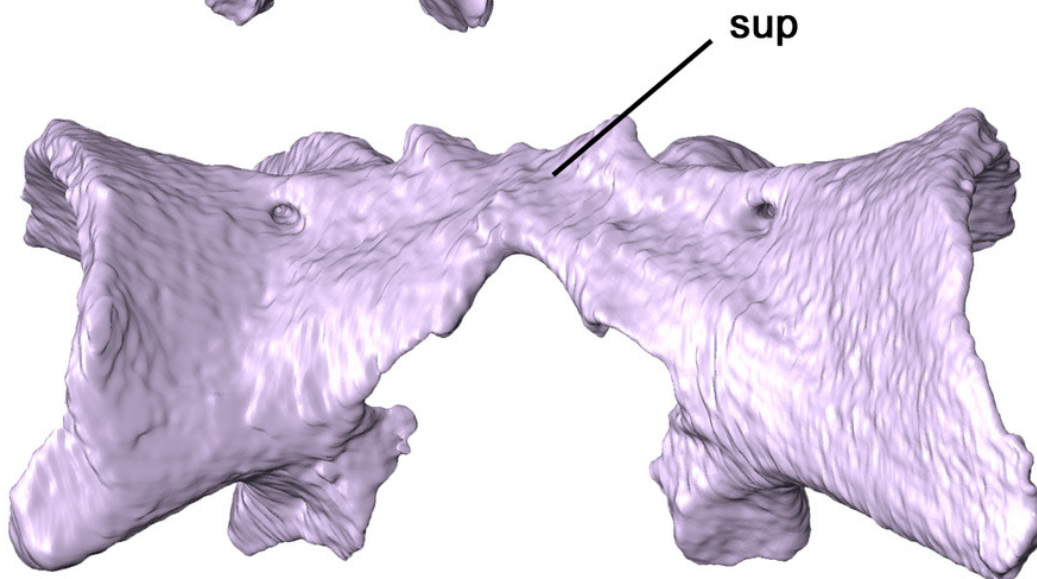
Figure 9

Semicircular canals of *Delorhynchus cifellii,* OMNH 73515.

(A) Anterior view, (B) lateral view and (C) occipital view of neurocranium, (D) anterior view, (E) lateral view, (F) dorsal view and (G) occipital view of left semicircular canals. Abbreviations: aasc = ampulla of anterior semicircular canal, alsc = ampulla of lateral semicircular canal, asc = anterior semicircular canal, cc = common crus, lsc = lateral semicircular canal, op = opisthotic, par = paroccipital process of opisthotic, pro = prootic, psc = posterior semicircular canal, sup = supraoccipital, vs = vestibule.

A

sup

B

pro

op

C

sup

op

D

asc

E

aasc

cc

cc

psc

aasc

alsc

psc

lsc

vs

alsc

lsc

vs

F

alsc

asc

cc

lsc

psc

G

aasc

asc

alsc

cc

lsc

psc

vs

5 mm
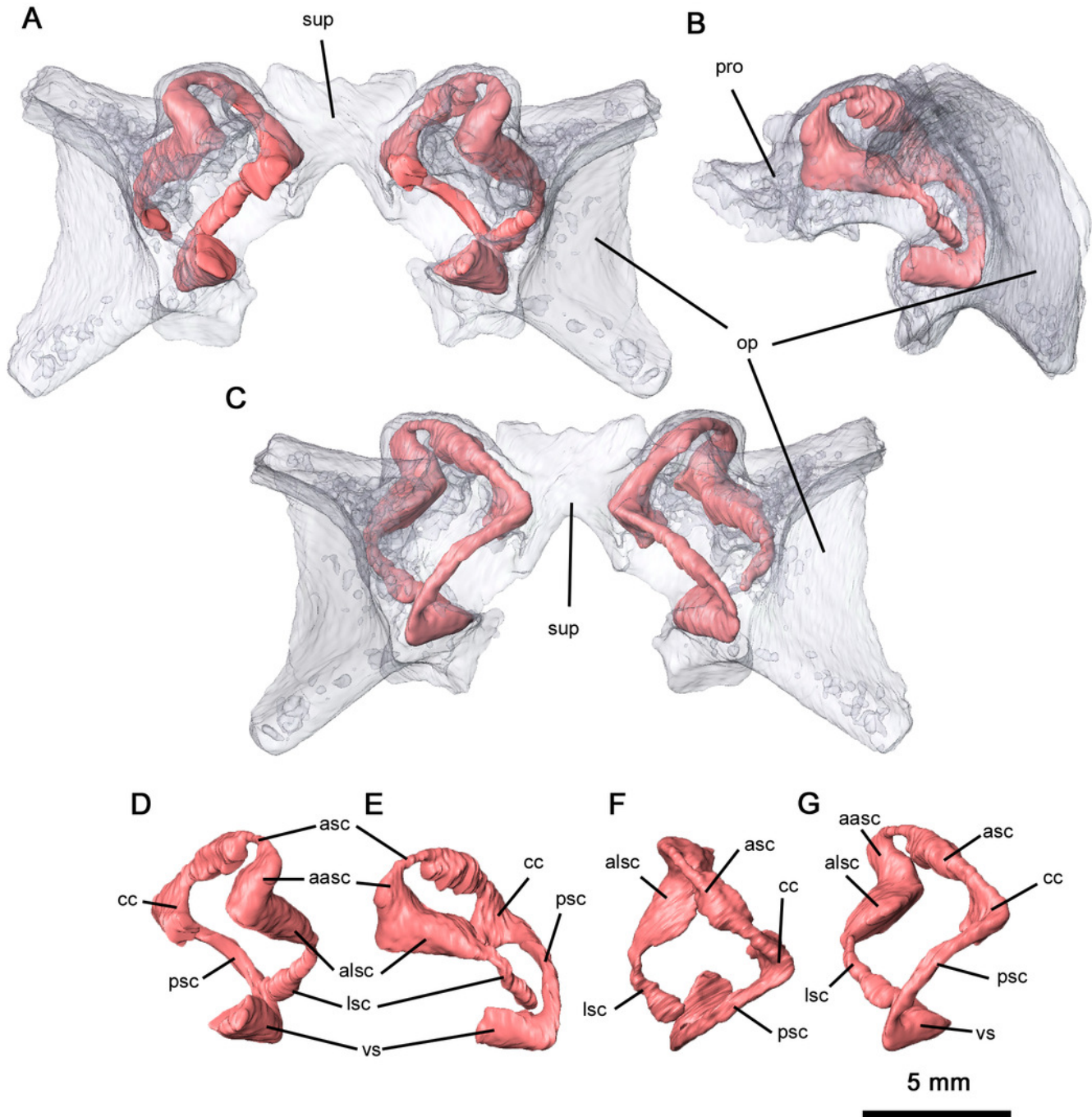
Figure 10

Mandible of *Delorhynchus cifellii,* OMNH 73515.

(A) Dorsal view of mandible, (B) medial view of right mandible and (C) lateral view of right mandible. Abbreviations: an = angular, art = articular, cr1 = first coronoid ossification, cr2 = second coronoid ossification, d = dentary, p. Mck. f. = posterior Meckelian fossa, pra = prearticular, sur = surangular.
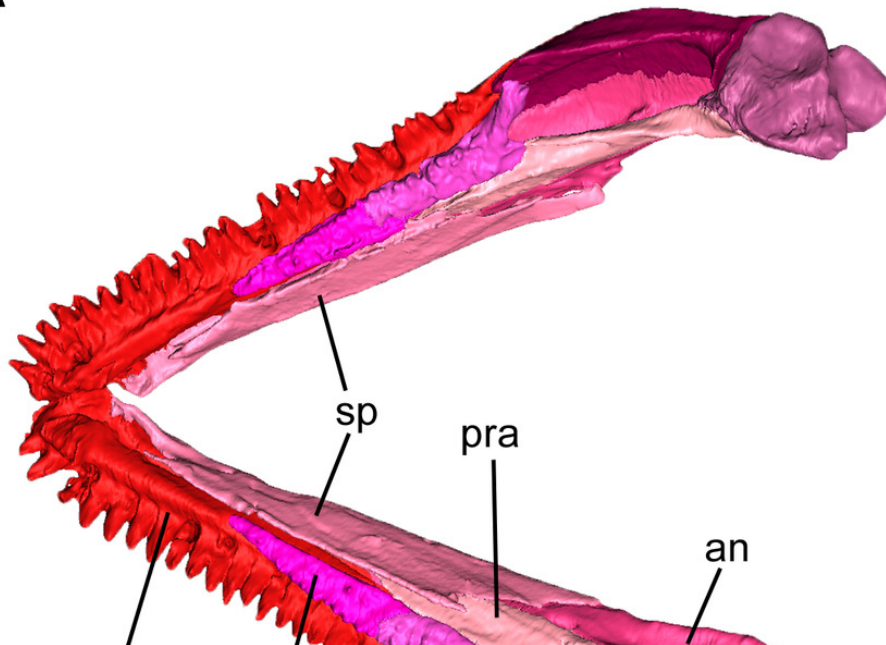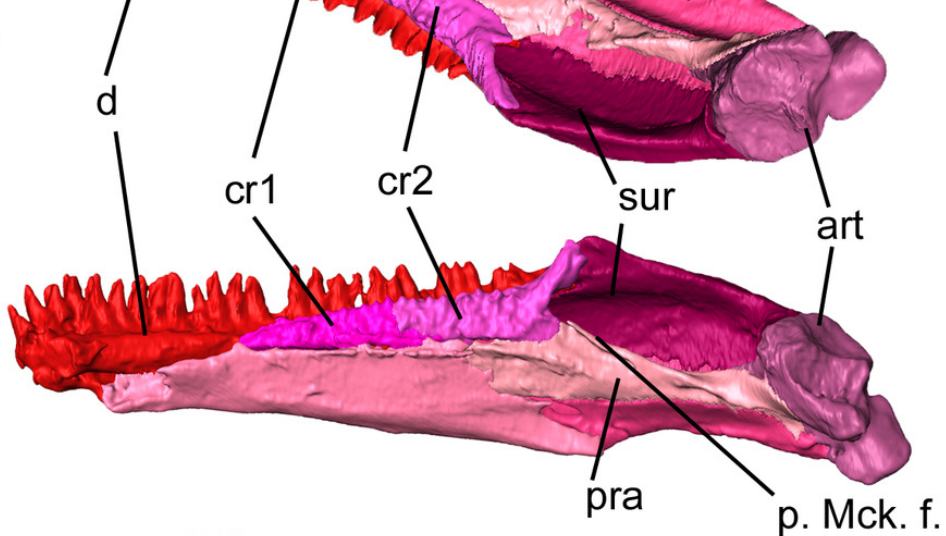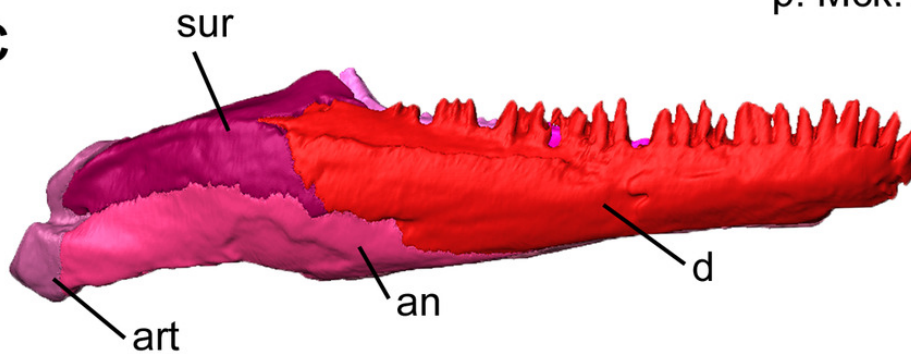
Figure 11

Representative vertebrae of *Delorhynchus cifellii,* OMNH 73515 in anterior, lateral, dorsal, and ventral views.

(A) Axis vertebra, (B) third cervical vertebra, (C) sixth cervical vertebra and (D) anterior dorsal vertebra.
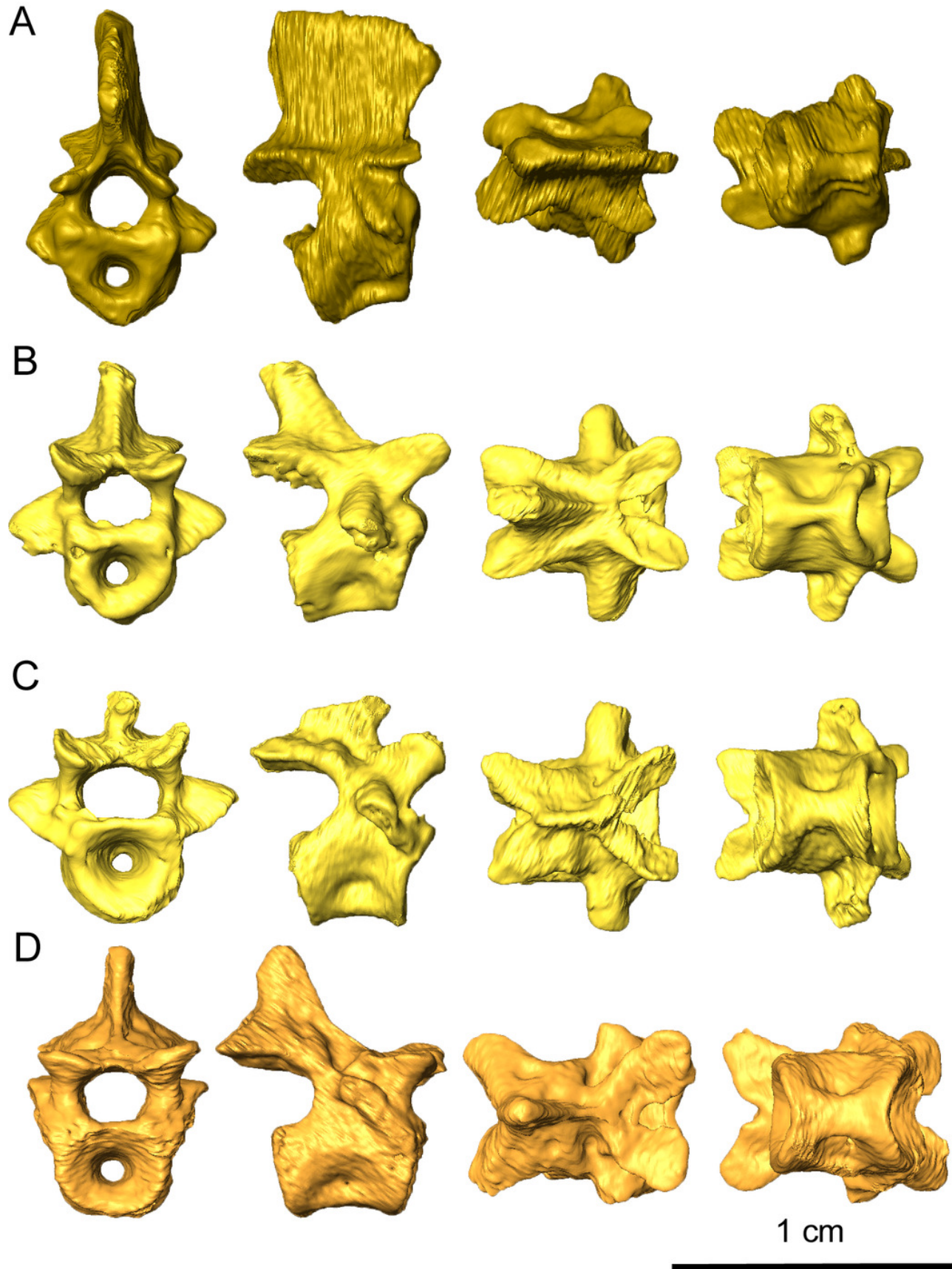
A

B

C

D

1 cm

Figure 12

Shoulder girdle elements of *Delorhynchus cifellii,* OMNH 73515.

(A) Lateral view and (B) medial view of left clavicle, (C) dorsal and (D) ventral views of interclavicle, (E) lateral view and (F) medial view of left scapulocoracoid. Abbreviations: gl = glenoid, gl. for. = glenoid foramen, sg. for. = supraglenoid foramen.
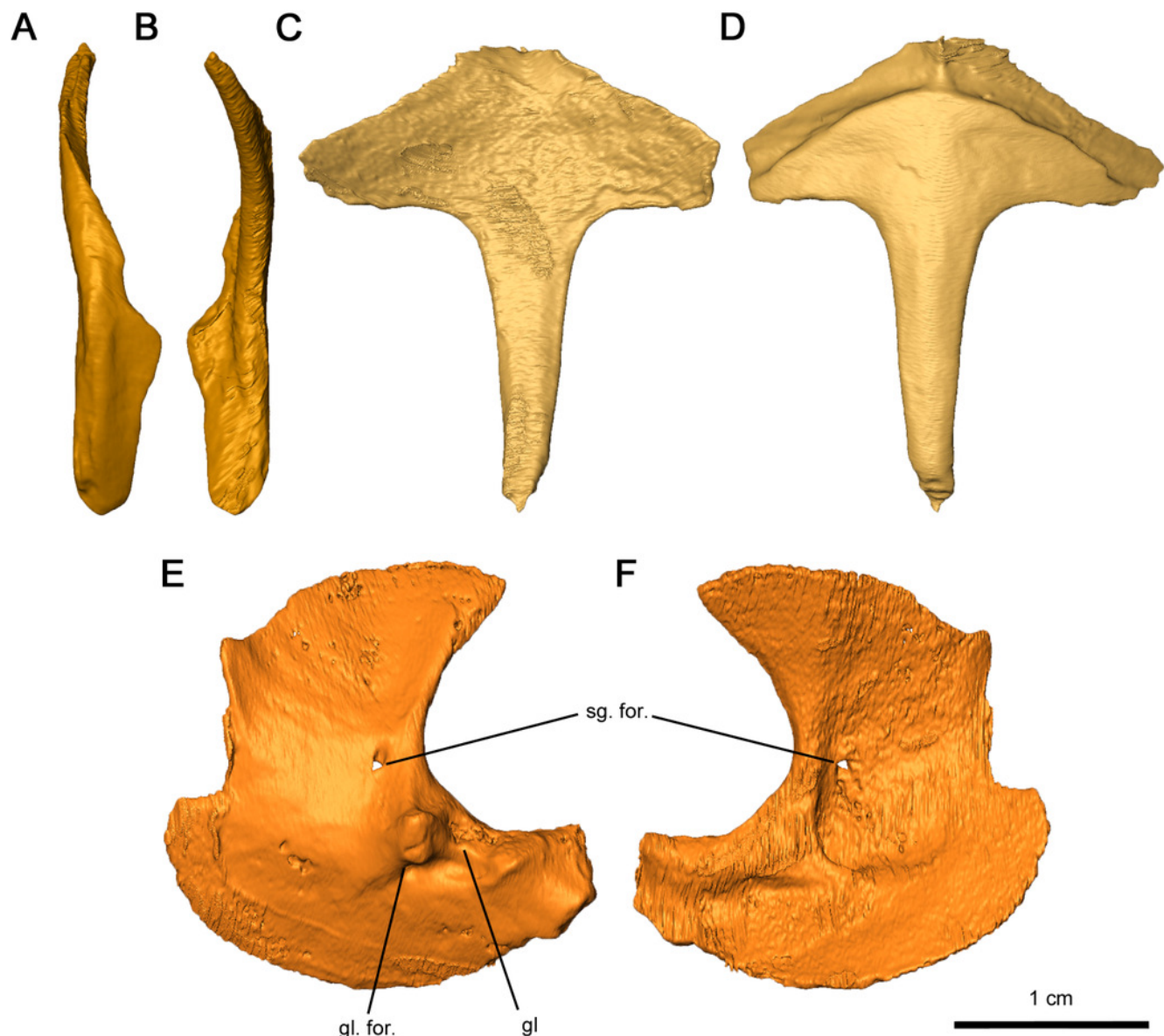
Figure 13

Left humerus of OMNH 73515.

(A) Proximal dorsal, (B) proximal ventral, (C) distal dorsal, (D) distal ventral, (E) proximal end and (F) distal views. Abbreviations: cap = capitulum, dpc = deltopectoral crest, ectp = ectepicondyle, ectp. for. = ectepicondylar foramen, entp = entepicondyle, entp. for. = entepicondylar foramen, l. dor. att. = attachment point of latissimus dorsi, sup. pr. = supinator process, tro = trochlea.
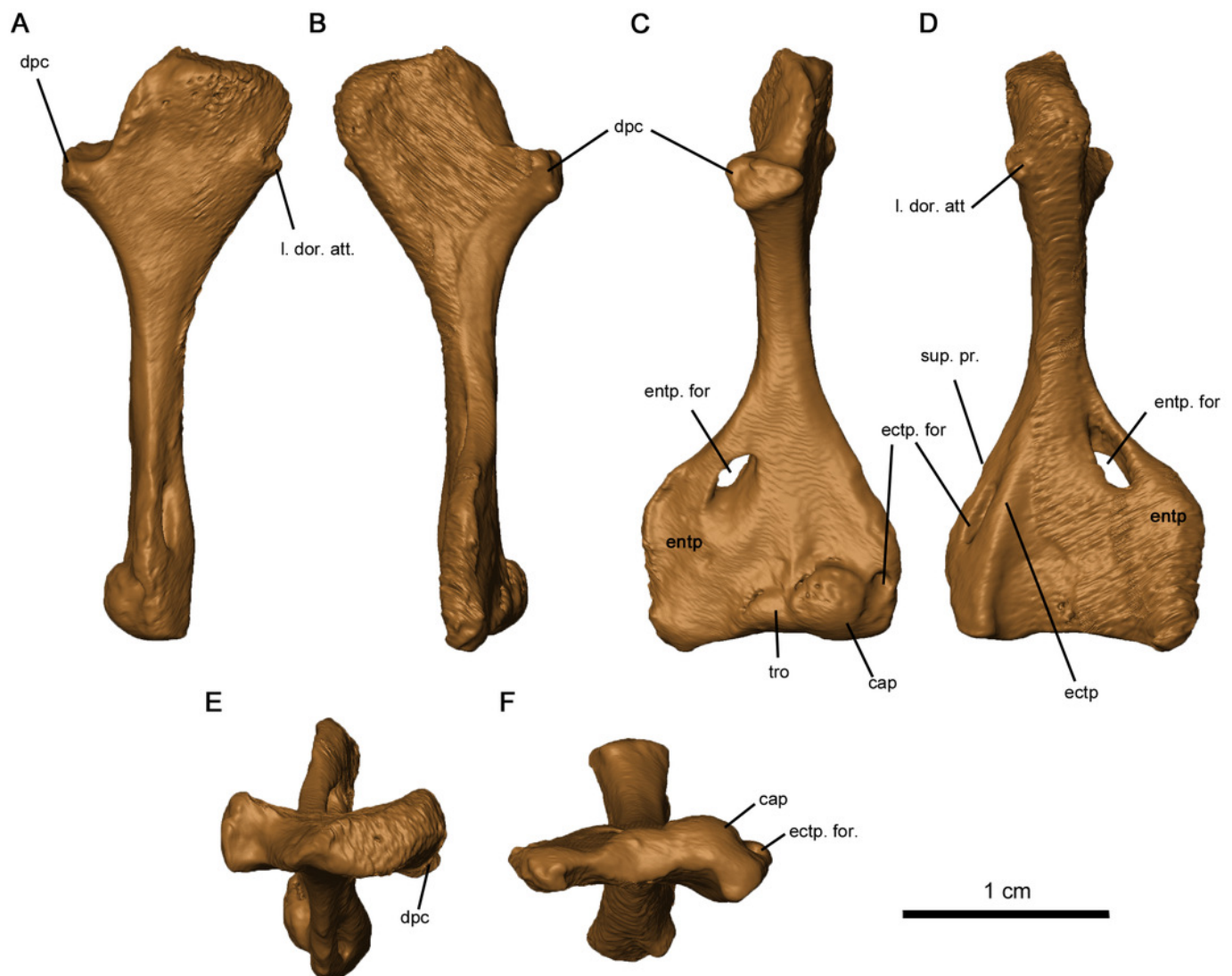
Figure 14

Strict consensus of 2 most parsimonious cladograms of parareptile relationships (length 878 steps).

Bootstrap values (>50%) have been provided before the nodes.